Monthly Notices
of the
ROYAL ASTRONOMICAL SOCIETY

MNRAS **493,** 1063–1087 (2020)
Advance Access publication 2020 January 14

doi:10.1093/mnras/staa039

The High Time Resolution Universe Pulsar Survey – XVI. Discovery and timing of 40 pulsars from the southern Galactic plane

A. D. Cameron [1,2★] D. J. Champion [1] M. Bailes,[3,4] V. Balakrishnan,[1] E. D. Barr [1,4] C. G. Bassa,[5] S. Bates,[6] S. Bhandari,[2] N. D. R. Bhat,[7] M. Burgay [8] S. Burke-Spolaor,[9] C. M. L. Flynn,[3] A. Jameson,[3,4] S. Johnston [2] M. J. Keith,[6] M. Kramer,[1,6] L. Levin,[6] A. G. Lyne,[6] C. Ng [10] E. Petroff [5] A. Possenti,[8,11] D. A. Smith,[12] B. W. Stappers,[6] W. van Straten [13] C. Tiburzi[1,14] and J. Wu[1]

Affiliations are listed at the end of the paper

Accepted 2019 December 29. Received 2019 December 17; in original form 2019 October 1

ABSTRACT

We present the results of processing an additional 44 per cent of the High Time Resolution Universe South Low Latitude (HTRU-S LowLat) pulsar survey, the most sensitive blind pulsar survey of the southern Galactic plane to date. Our partially coherent segmented acceleration search pipeline is designed to enable the discovery of pulsars in short, highly accelerated orbits, while our 72-min integration lengths will allow us to discover pulsars at the lower end of the pulsar luminosity distribution. We report the discovery of 40 pulsars, including three millisecond pulsar-white dwarf binary systems (PSRs J1537−5312, J1547−5709, and J1618−4624), a black-widow binary system (PSR J1745−23) and a candidate black-widow binary system (PSR J1727−2951), a glitching pulsar (PSR J1706−4434), an eclipsing binary pulsar with a 1.5-yr orbital period (PSR J1653−45), and a pair of long spin-period binary pulsars which display either nulling or intermittent behaviour (PSRs J1812−15 and J1831−04). We show that the total population of 100 pulsars discovered in the HTRU-S LowLat survey to date represents both an older and lower luminosity population, and indicates that we have yet to reach the bottom of the luminosity distribution function. We present evaluations of the performance of our search technique and of the overall yield of the survey, considering the 94 per cent of the survey which we have processed to date. We show that our pulsar yield falls below earlier predictions by approximately 25 per cent (especially in the case of millisecond pulsars), and discuss explanations for this discrepancy as well as future adaptations in RFI mitigation and searching techniques which may address these shortfalls.

Key words: surveys – stars: neutron – pulsars: general.

1 INTRODUCTION

The ongoing search for new pulsars remains a core goal of current efforts in pulsar astronomy. Although the ATNF Pulsar Catalogue[1] (PSRCAT, Manchester et al. 2005) already lists approximately 2800 pulsars, the body of which have allowed for enormous progress in our understanding of multiple areas of physics, it is largely by the discovery of new pulsars that our understanding is extended. New discoveries help complete our knowledge of the underlying pulsar population, and the more unusual and exotic of these new pulsars present new physical challenges to be explored and explained.

We have therefore undertaken the High Time Resolution Universe South Low Latitude (HTRU-S LowLat) pulsar survey, a long-integration, high time resolution blind pulsar survey of the southern Galactic plane region taken with the 21-cm multibeam receiver (MB20; Staveley-Smith et al. 1996) of the Parkes 64-m Radio Telescope. The survey is one component of the HTRU-South all-sky pulsar survey (HTRU-S; Keith et al. 2010), which fully covers the region of sky below a declination of $\delta < +10°$. The three components of this survey are divided into regions of Galactic longitude l and latitude b, giving the high-, mid-, and low-latitude survey regions, with the design of each survey tailored towards specific scientific objectives. HTRU-S is complemented by a corresponding northern survey, HTRU-North (HTRU-N; Barr et al. 2013), undertaken with the Effelsberg 100-m Radio Telescope.

★ E-mail: andrew.cameron@csiro.au
[1] http://www.atnf.csiro.au/people/pulsar/psrcat/

While the general goal of any pulsar survey can largely be characterized as the discovery of new pulsars, the primary goal of HTRU-S LowLat has been the discovery of relativistic binary pulsars. These binary systems can serve as excellent laboratories for developing tests of gravitational theories such as general relativity (GR), with the Double Pulsar PSR J0737−3039 (Burgay et al. 2003; Lyne et al. 2004; Kramer et al. 2006b) currently standing as the leading example of such a gravitational laboratory. The region of sky surveyed by HTRU-S LowLat (between Galactic longitudes of $-80^\circ < l < 30^\circ$ and Galactic latitudes $|b| < 3.5^\circ$) comprises the densest portion of the Galactic plane, and is expected to contain the highest proportion of these systems (Belczynski, Kalogera & Bulik 2002). Compact binary systems with short orbital periods ($P_b < 12$ h) are of particular interest, as these systems are likely to display the most significant relativistic effects, allowing for new and improved tests and limits well beyond those available from current binary pulsars.

An important secondary goal of the survey involves the discovery of low-luminosity pulsars too weak to have been detected by earlier pulsar surveys. This is made possible by the 72-min observations employed by HTRU-S LowLat. Significant effort has been spent attempting to model the luminosity distribution function of pulsars both within and outside the Galactic plane (see e.g. Faucher-Giguère & Kaspi 2006; Levin et al. 2013; Bates et al. 2014; Gullón et al. 2014; Gonthier et al. 2018; Cieślar, Bulik & Osłowski 2020), as well as to link this distribution to other aspects of pulsar phenomenology (e.g. spin periods and spin-period derivatives). However, such efforts are intrinsically constrained by those pulsars which are currently known and available for study. Further characterizing the population statistics of low-luminosity pulsars will allow for a greater understanding of the pulsar population as a whole, and will be vital in the planning of future pulsars surveys to be undertaken with next-generation radio telescopes such as MeerKAT,[2] the Square Kilometre Array[3] (SKA), and the Five-hundred-meter Aperture Spherical Telescope[4] (FAST), which are likely to probe even deeper into this regime. Finally, the long observation times are also favourable for capturing various transient radio phenomena, including rotating radio transients (see e.g. McLaughlin et al. 2006; Keane et al. 2010), both nulling and intermittent pulsars, and potentially fast radio bursts (see e.g. Lorimer et al. 2007; Thornton et al. 2013; Champion et al. 2016).

The HTRU-S LowLat survey has already made a significant scientific contribution to each of these scientific goals, and this paper marks its third major discovery publication. Ng et al. (2015) reported the discovery of 60 pulsars in the first 50 per cent of the survey to be processed, along with the specifications of the 'partially coherent segmented acceleration search' pipeline used to analyse the data (further described in Section 2). The reported population of pulsars were of lower luminosity than the background population from the survey region and, in the case of the un-recycled pulsars, appeared to represent a typically older population. Ng et al. (2015) also reported four binary pulsars (PSRs J1101−6424, J1244−6359, J1755−25, and J1759−24) and two nulling pulsars (PSRs J1227−63 and J1349−63), demonstrating HTRU-S LowLat's ability to discover both binary systems and transient phenomena. Meanwhile, continued processing of the remaining portion of the survey with the same search pipeline resulted in the discovery of PSR J1757−1854 as reported in Cameron et al. (2018), the most accelerated binary pulsar currently known and the only relativistic binary pulsar to have been discovered in the entire HTRU-S survey thus far.

This paper presents new results derived from the processing of an additional 44 per cent of the HTRU-S LowLat survey through the 'partially coherent segmented acceleration search' as described in Ng et al. (2015), including the discovery of a further 40 pulsars.[5] This brings the total fraction of the survey processed through this pipeline to 94 per cent. Section 2 summarizes the search strategy used in the processing of the survey data, and the current status of the survey processing. Section 3 discusses the redetections of known pulsars within the processed 44 per cent of the survey data. Section 4 presents the details of the newly discovered pulsars, including timing solutions where available. Section 5 then follows up with an in-depth discussion of a selection of pulsars of interest. Section 6 provides an analysis of the survey discoveries within the context of the larger pulsar population, with an evaluation of the survey yield presented in Section 7. Additional discussion and conclusions follow in Section 8.

2 METHODOLOGY

The 'partially coherent segmented acceleration search' pipeline used to process the 44 per cent of the HTRU-S LowLat survey analysed for this paper (as well as the subsequent pulsar candidate identification and confirmation procedures) are the same as those described by Ng et al. (2015). For completeness, we present here a brief summary of this technique.

In order to allow for the detection of binary pulsars, our pipeline employs the 'time-domain resampling' acceleration search technique (see e.g. Middleditch & Kristian 1984; Johnston & Kulkarni 1991). This technique assumes that the orbital motion of a pulsar can be modelled by a constant acceleration a over the span of a given observation such that the line-of-sight velocity can be expressed by $V(t) = at$. If this assumption remains true (i.e. that the 'jerk' or rate of change of acceleration $\dot{a} \simeq 0\,\mathrm{m\,s^{-3}}$), then each dedispersed time series [up to a maximum dispersion measure (DM) of 3000 $\mathrm{cm^{-3}}$ pc] can be quadratically resampled so as to remove the effect of the orbital motion over the course of the observation. This technique works best (in the case of circular orbits) when the parameter

$$r_{\mathrm{orb}} = \frac{t_{\mathrm{int}}}{P_{\mathrm{b}}} \lesssim 0.1, \tag{1}$$

where t_{int} is the integration time of the observation and P_{b} is the orbital period of the pulsar. This value of r_{orb} is based on an in-depth investigation detailed in appendix A1 of Ng et al. (2015).

The integration time of each observation is $t_{\mathrm{int}} = 4300$ s, which by equation (1) implies a sensitivity to $P_{\mathrm{b}} \gtrsim 12$ h. In order to optimize the sensitivity of each observation to shorter orbital periods, we adopt a segmented search strategy. Each observation is broken into full-length ($s = 1$), half-length ($s = 2$), quarter-length ($s = 4$), and eighth-length ($s = 8$) segments, resulting in 15 segments in total. Each group of segments spans the entire full-length observation without overlap. This segmenting provides sensitivity to progressively shorter orbital periods, with the t_{int} of each segment and its optimal P_{b} range described in Table 1. However, with each additional halving of the observation length

[2] http://www.ska.ac.za/science-engineering/meerkat/
[3] http://skatelescope.org/
[4] http://fast.bao.ac.cn/en/

[5] This total includes the previously published PSR J1757−1854, which is included here as it was discovered as part of survey processing presented in this paper.

Table 1. A summary of the 15 individual segments searched as part of the partially coherent segmented acceleration search, including the number of segments (s) in each group, the minimum orbital period (P_b) to which each is sensitive and their acceleration search ranges ($|a_{min}|$ to $|a_{max}|$).

Segment	s	t_{int} (s)	Min. P_b (h)	$\lvert a_{min}\rvert$ ($m\,s^{-2}$)	$\lvert a_{max}\rvert$ ($m\,s^{-2}$)
Full-length	1	4300	12	0	1
Half-length	2	2150	6	0	200
Quarter-length	4	1075	3	200[a]	500
Eighth-length	8	537	1.5	0	1200

Note. [a]A minority of the processed data was also searched within $|a| < 200\,m\,s^{-2}$ in the $s = 4$ segment.

t_{int}, the flux–density sensitivity of the segments correspondingly lowers by a factor of $\sqrt{2}$. Our strategy aims to strike an ideal balance between these two considerations, optimizing our ability to detect binary systems with small values of P_b while retaining as much of the observation length and therefore as much sensitivity as possible. Each of the 15 segments of a given observation beam is searched coherently through an acceleration and Fourier search, but is processed independently to each of the other segments, hence rendering the pipeline only 'partially coherent'.

Acceleration search ranges for the $s = 2, 4, 8$ segments are chosen by adopting a hypothetical neutron star-black hole (NS-BH) binary scenario as a limiting case. Assuming a circular orbit with a $1.4\,M_\odot$ NS and a $10\,M_\odot$ BH and using the minimum P_b to which each segment is sensitive, we derive limiting acceleration values using Kepler's third law

$$|a_{max}| = \left(\frac{2\pi}{P_b}\right)^{4/3} (T_\odot f)^{1/3}\, c, \tag{2}$$

where c is the speed of light, $T_\odot$ is defined as

$$T_\odot = \frac{GM_\odot}{c^3} = 4.925\,490\,947\,\mu s, \tag{3}$$

where G is Newton's gravitational constant, and f is the mass function as defined by

$$f = \frac{(m_c \sin i)^3}{(m_c + m_p)^2}, \tag{4}$$

where m_p and m_c are the mass of the pulsar and the companion, respectively, both in units of $M_\odot$. These acceleration ranges are also listed in Table 1. Meanwhile, the comparably narrow acceleration search range adopted for the full-length $s = 1$ segment is intended to optimize sensitivity to mildly accelerated binary systems in wider orbits. Our choice of acceleration search step size for each segment is adopted from Eatough et al. (2013).

2.1 Candidate selection and confirmation

In a 'conventional' survey, pulsar candidates are typically selected for further inspection if their spectral signal-to-noise ratio (S/N) is greater than a threshold value of S/N_{min}. The appropriate value of S/N_{min} can normally be derived using an assessment of the false-alarm statistics with respect to the number of dependent trials (see e.g. Lorimer & Kramer 2005). However, in the case of the partially coherent segmented acceleration search, this method is complicated by the multiple-pass, segmented nature of the search, which involves different numbers of both dependent and independent trials. As a conservative assessment, we have calculated the S/N_{min} for each iteration of the segmented search ($s = 1, 2, 4, 8$), considering only the number of dependent trials. From this, we derive a lower limit of $S/N_{min} \simeq 9.3$. We note that this value is likely to be an underestimate, as it fails to consider the complete search-space of the pipeline simultaneously, as well as the presence of radio frequency interference (RFI) which will raise the survey's noise floor.

However, given that erring towards a lower value of S/N_{min} is generally preferable, we conservatively consider each pulsar candidate produced by the pipeline with a spectral S/N > 8. Each of these candidates is then folded, and those candidates whose folded S/N > 8 are then manually inspected by eye to assess the likelihood of the candidate representing a true pulsar discovery. Promising candidates are then reobserved with the Parkes 64-m Radio Telescope to confirm them as pulsars should they be redetected. Once confirmed, regular timing observations of each pulsar are conducted with a cadence of approximately 1 month, supplemented by intervals of higher cadence observations as required to obtain a phase-connected solution. Those pulsars with declinations $\delta < -30^\circ$ are timed exclusively at Parkes, while those with $\delta > -30^\circ$ are typically passed to Jodrell Bank to be observed using the 76-m Lovell Radio Telescope.

Our confirmation strategy follows that of Ng et al. (2015), and involves reobserving each candidate using a 'Ring-of-3' set of grids (labelled A–B–C) in a triangular configuration, each offset from the central discovery position (Grid D) by $\sim 0.139^\circ$ such that they are separated from each other by the full width at half-maximum (FWHM) of the MB20 receiver (0.24°). Typically, each of these grids is observed in turn until the pulsar is redetected, using a reduced t_{int} designed to redetect the candidate pulsar at approximately S/N = 10. If no redetection is made in any of the offset grids (A–B–C), additional confirmation observations may be taken at the discovery position (D). If available, archival data from the Parkes Multibeam Pulsar Survey (PMPS; Manchester et al. 2001) as well as data from the HTRU-S Medium Latitude survey (HTRU-S MedLat; Keith et al. 2010) may also be searched to obtain additional information regarding the position and timing properties of the new pulsar.

2.2 Status of survey processing

Of the 1230 scheduled pointings which comprise HTRU-S LowLat, 536 ($\sim$ 44 per cent) have been processed through the partially coherent segmented acceleration search as part of this paper. This is in addition to the 618 pointings ($\sim$ 50 per cent) which were previously processed by Ng et al. (2015), of which 180 ($\sim$ 15 per cent) have only been processed through a 'standard', non-acceleration search (for details, see Keith et al. 2010). A further 51 pointings encountered an error during processing, either due to data corruption or an error in the operation of the pipeline, in which case they may yet be recoverable by future processing efforts. In total, these 1205 pointings account for $\sim$ 98 per cent of the entire HTRU-S LowLat pulsar survey,[6] with $\sim$ 94 per cent having been successfully processed and reviewed.

3 KNOWN PULSAR REDETECTIONS

In order to verify that the processing pipeline achieved the expected sensitivity, a complete record of the expected redetections of

[6]The pointings accounting for the remaining 2 per cent of the survey could not be processed as their data was unavailable for recall.

previously known pulsars in the survey region has been maintained, following the same procedure as outlined in Ng et al. (2015). For each survey beam, the current PSRCAT parameters of each nearby pulsar, including the pulsar's spin period P, its effective pulse width $W_{\rm eff}$ (which we approximate as W_{50}, the width of the pulse at 50 per cent of its peak value) and its flux density at 1.4 GHz, S_{1400} were recorded. For those pulsars for which a W_{50} is not recorded, a conservative value of W_{50} was assumed. Due to the non-uniform response of each telescope beam, any offset of the pulsar from the centre of the beam will cause a reduction in its apparent flux density, and correspondingly a reduction in its measured S/N. In order to account for this, we approximate the response pattern of the telescope beam as a Gaussian curve and calculate the expected apparent flux density:

$$S_{\rm exp} = S_{1400}\, {\rm e}^{-\theta^2/2\sigma^2}, \tag{5}$$

where θ is the offset in degrees and σ is related to the FWHM of the telescope beam by

$$\sigma = \frac{\rm FWHM}{2\sqrt{2\ln 2}}. \tag{6}$$

With each beam of the Parkes MB20 receiver having an FWHM of approximately 0.24°, this results in $\sigma \simeq 0.1^\circ$. Based upon the modified value of $S_{\rm exp}$, the expected S/N ($\rm S/N_{exp}$) is then derived using the radiometer equation:

$$\rm S/N_{exp} = \left(\frac{S_{exp} G \sqrt{n_p t_{int} \Delta f}}{\beta T_{sys}}\right)\left(\frac{P - W_{50}}{W_{50}}\right)^{1/2}, \tag{7}$$

where G is the telescope gain in K Jy^{-1} and varies between 0.735, 0.69, and 0.581 for the central, inner, and outer beams of the receiver (see table 3 of Keith et al. 2010). Meanwhile, the 'degradation factor' $\beta \simeq 1.16$, the effective bandwidth of the receiver $\Delta f = 340$ MHz, and the system temperature $T_{\rm sys} = T_{\rm sky} + T_{\rm rcvr}$, where $T_{\rm sky} \simeq 7.6$ K (a mean value for the survey region, see table 4 of Keith et al. 2010) and $T_{\rm rcvr} \simeq 23$ K. For our observations, the number of polarizations $n_{\rm p} = 2$ and the integration time $t_{\rm int} = 4300$ s.

We report 755 individual redetections of 390 unique pulsars from the reported 44 per cent of the HTRU-S LowLat survey. A full record of these 755 redetections can be found in Appendix A1. Considering all HTRU-S LowLat survey data processed to date, this results in 1667 redetections spanning a combined total of 649 unique pulsars.[7]

Fig. 1 shows a comparison of the calculated $\rm S/N_{exp}$ against the measured S/N ($\rm S/N_{obs}$) for a subset of the 755 pulsar redetections reported here. As the response pattern of the telescope beam deviates from our Gaussian approximation outside of the beam FWHM, all redetections with an offset $\theta >$ FWHM/2 $= 0.12^\circ$ (totalling 434 redetections) have been excluded from this comparison. Also excluded are two redetections of pulsars without a recorded S_{1400}, for which $\rm S/N_{exp}$ cannot be calculated. Finally, 93 redetections are excluded due to the position of the relevant survey beams being sufficiently ambiguous to prevent an accurate determination of θ and hence allow for an accurate determination of $\rm S/N_{exp}$. This ambiguity appears to have been caused by an error in the recorded position of each beam at the time the survey was taken, affecting the header information of the recorded files. In total, after accounting for these caveats, 226 pulsar redetections remain for the purposes of this analysis.

As shown in Fig. 1, a significant majority of redetections fall close to the 1:1 relation as expected. However, the division of data points around this relation does not appear to be symmetric, with 163 redetections (approximately 72 per cent) having $\rm S/N_{exp} > S/N_{obs}$. As noted by both Keith et al. (2010) and Ng et al. (2015), this is likely to be partly due to a reporting bias, where the highest values of S/N observed during each known pulsar's initial set of observations tend to be reported (the variation in S/N between observations being due to scintillation and other potential instrumental effects, as further discussed in Levin et al. 2013). This leads to higher catalogue values of S_{1400} which in turn leads to higher values of $\rm S/N_{exp}$. The potential effect of scintillation can be seen in panel (a) of Fig. 1, which plots the ratio of $\rm S/N_{exp}/S/N_{obs}$ as a function of catalogue DM. The scatter of redetections is seen to increase towards lower DM values where the effects of scintillation are likely to be most prominent (see e.g. Sutton 1971; Backer 1975).

Another contributing factor to the observed scatter seen in Fig. 1 is our choice of a constant value of $T_{\rm sky}$ in calculating $\rm S/N_{exp}$. In reality, the value of $T_{\rm sky}$ typically increases with decreasing absolute Galactic latitude ($|b|$), which would cause an additional overestimation of $\rm S/N_{exp}$ at the lowest values of $|b|$ (Haslam et al. 1981). This effect is clearly seen in panel (b) of Fig. 1, where the red line shows the median of the $\rm S/N_{exp}/S/N_{obs}$ scatter as a function of b, clearly peaking close to $b = 0^\circ$.

3.1 Non-detections of known pulsars

We also note a number of non-detections of known pulsars expected to be detectable above a threshold folded S/N ($\rm S/N_{min}$). For this analysis we set $\rm S/N_{min} = 9$ to maintain consistency with the previous work conducted in Ng et al. (2015). In addition, we again restrict our analysis to those non-detections with an offset $\theta \leq 0.12^\circ$ and whose beam position is unambiguous.

Under these criteria, we identify 21 non-detections spanning 21 unique pulsars. We note that none of these 21 pulsars are known to be in binary systems. At present, we are able to account for 12 of the non-detections, with 9 remaining unexplained. Details of these non-detections are given in Appendix A2.

Considering these non-detected pulsars in comparison to the set of redetected pulsars, we calculate that ~ 2 per cent of expected pulsars have been missed during the processing of the ~ 44 per cent of the HTRU-S LowLat survey data processed in this paper. This is comparable with the ~ 1 per cent non-detection rate reported for the ~ 50 per cent processed by Ng et al. (2015), indicating that the more recently processed data has been analysed to an approximately equivalent sensitivity.

3.2 Binary redetections

As the goal of the partially coherent segmented acceleration search pipeline is to enhance our sensitivity to binary pulsars, we have also maintained a record of the observed S/N of each redetected binary pulsar across each searched segment. A total of 17 unique binary pulsars were detected across 28 individual survey beams. The highest S/N redetections and detected accelerations of each pulsar across all segments are provided in Appendix A3. As indicated by the listed values of $P_{\rm b}$, the majority of these pulsars (up to and including PSR J1431−5740) are of sufficiently long orbital periods so as to be easily detectable without the need for a segmented

[7]This number is less than the sum of the totals from each portion of the survey due to the mutual overlap in the sets of individual pulsars detected in each half.

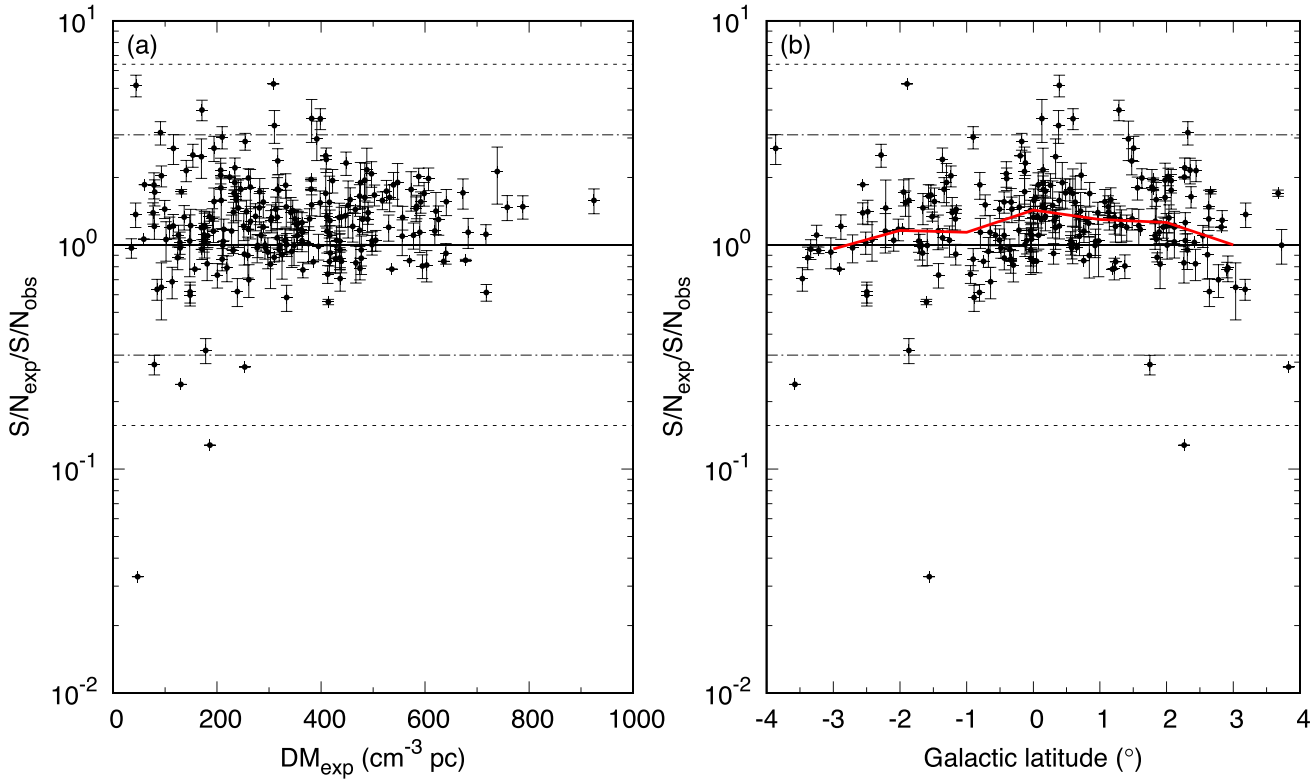

Figure 1. A comparison of the expected versus observed S/N values (S/N_{exp} and S/N_{obs}, respectively) for pulsars redetected in 44 per cent of the HTRU-S LowLat survey. Panel (a) shows $S/N_{exp}/S/N_{obs}$ plotted against the PSRCAT DM for each redetected pulsar, while panel (b) shows $S/N_{exp}/S/N_{obs}$ plotted as a function of each pulsar's Galactic latitude. The bold line in each case represents the 1:1 relation, while the surrounding dashed lines extending outwards from the 1:1 line indicate contours containing 95 per cent and 99 per cent of the redetections, respectively. The red line in panel (b) shows the median of the scatter, determined using bins with a width of 1°.

acceleration search, and were typically detected at maximum S/N in the full-length observation.

More interesting behaviour is observed as P_b shrinks to the point where r_{orb} (as defined by equation 1) approaches 0.1 for the full-length observation (corresponding to a critical orbital period defined as $P_{b,crit} = 12$ h). Here we consider the examples of both PSR J1435−6100 ($P_b = 32.5$ h) and PSR J1802−2124 ($P_b = 16.8$ h). Although the orbital period of both pulsars is larger than $P_{b,crit}$, the maximum line-of-sight accelerations of both pulsars exceeds the $\pm 1\,m\,s^{-2}$ search range of the full-length segments (as listed in Table 1). This is likely a significant factor in the non-detection of either pulsar in the full-length segment, with each pulsar only being detected in shorter segments which were searched at larger acceleration values. This therefore appears to represent a parameter space to which our pipeline may not be sensitive. Pulsars with similar orbital parameters ($P_b > P_{b,crit}$ and $|a| > 1\,m\,s^{-2}$) but lower flux densities may not be detectable in the shorter segments, requiring the sensitivity of the full-length observation to be identified. However, as our search is specifically intended to target those pulsars for which $P_b < P_{b,crit}$, we do not consider this a great concern.

Additionally, the two beams in which PSR J1802−2124 was detected (as listed in Table A3) highlight the dependence of the search sensitivity on the orbital phase (φ) at which a given pulsar was observed. In beam 2011-12-30-23:14:07/02, PSR J1802−2124 experienced accelerations low enough for a near-optimal detection in the full-length observation. However, both the full-length and half-length segment detections in this beam show the presence of jerk ($\dot{a}$), which is at its maximum magnitude in a circular orbit when $a \simeq 0\,m\,s^{-2}$. It is at these orbital phases that the $r_{orb} \simeq 0.1$ approximation is least applicable, with a smaller r_{orb} being favoured (Ng et al. 2015). This contributes to the higher S/N detection seen in the half-length segment of 2011-12-30-23:14:07/02. In contrast, the detection of PSR J1802−2124 in beam 2011-10-12-04:24:15/07 occurs at an acceleration close to a_{max} where the jerk $\dot{a} \simeq 0$, and no evidence of jerk is seen in the half-segment detection.

Finally, PSR J1141−6545 represents the only known short-P_b, relativistic binary that was observed and redetected during this portion of the survey processing.[8] The pulsar experiences high line-of-sight accelerations[9] and is also moderately eccentric with $e = 0.17$, making it a unique test case for the segmented acceleration search pipeline. In all four beams in which the pulsar was detected, the maximum S/N detection occurred in the half-length segment, for which $r_{orb} = 0.13$. With an $r_{orb} = 0.06$, the quarter-length segments are also near-ideally suited to a detection of the pulsar, and had these segments been searched at smaller values of acceleration it is likely the detected S/N in these segments would have been consistent with the expected $\sqrt{2}$ reduction in S/N from the half-segment values. However, the stronger S/N of the half-segment detections

[8]One additional short-P_b, relativistic binary (PSR J1756−2251) exists within the HTRU-S LowLat survey region, but did not fall within any of the survey beams processed for this paper.

[9]The maximum and minimum line-of-sight accelerations of PSR J1141−6545 change over time due its high rate of periastron advance of $\dot{\omega} \simeq 5.31\,yr^{-1}$ (Bhat, Bailes & Verbiest 2008).

Table 2. For each of the 40 newly discovered pulsars from the HTRU-S LowLat survey, we list here the survey beam in which each pulsar was discovered (identified by its starting UTC time stamp and beam number), along with the S/N at which each pulsar was detected in the survey (S/N_{HTRU}) and, if available, the S/N of the pulsar in the PMPS (S/N_{PMPS}). Also listed are the mean flux density (S_{1400}), pulse widths at 50 per cent and 10 per cent of the pulse peak (W_{50} and W_{10}) and derived luminosity (L_{1400}) of each pulsar. Values in parentheses, where available, represent 1σ uncertainties on the final digit. L_{1400} is based on the DM distance estimates to each pulsar, using the NE2001 model (left column; Cordes & Lazio 2002) and the YMW16 model (right column; Yao, Manchester & Wang 2017).

PSR name	Pointing/beam	S/N_{HTRU}	S/N_{PMPS}	S_{1400} (mJy)	W_{50} (ms)	W_{10} (ms)	L_{1400} (mJy kpc^2)	
J1136−6527	2012-02-18-20:27:49/12	11.8	–	0.14(2)	19.6	35.8	1.6	0.5
J1210−6322	2011-10-10-20:41:56/08	11.6	<7.0	0.151(15)	66.0	116.0	18.0	13.8
J1223−5856	2012-01-19-13:30:00/04	34.9	–	0.377(12)	63.3	85.5	10.6	8.6
J1300−6602	2012-02-18-21:41:30/01	13.5	<7.0	0.119(15)	22.1	96.3	21.5	28.9
J1344−5855	2011-12-28-17:24:43/04	15.4	8.2	0.138(10)	13.0	23.8	5.8	7.9
J1430−5712	2012-01-19-16:45:38/01	13.2	–	0.092(16)	10.0	39.8	0.81	1.4
J1434−5943	2011-12-27-16:36:22/08	13.3	<6.3	0.17(2)	42.9	55.6	0.94	1.7
J1504−5659	2011-12-13-18:40:47/05	14.2	7.5	0.11(2)	49.0	60.3	6.0	14.1
J1507−5800	2012-04-10-11:32:06/09	11.1	8.2	0.20(3)	8.70	64.5	7.5	7.0
J1513−6013	2012-07-21-06:33:26/08	18.0	8.9	0.20(4)	35.3	64.2	6.5	12.4
J1514−5316	2011-12-21-23:02:36/02	10.2	9.4	0.147(18)	5.16	16.1	0.1	0.1
J1537−5312	2011-12-23-18:06:55/08	14.8	9.3	0.458(15)	1.84	2.35	3.8	4.3
J1547−5709	2011-12-12-20:12:12/03	17.5	–	0.34(2)	0.149	0.905	1.2	2.5
J1557−5151	2011-12-08-04:31:54/12	17.2	<7.5	0.310(18)	28.9	63.5	23.3	13.0
J1603−5312	2012-08-03-05:51:26/09	14.0	9.0	0.25(5)	24.4	45.9	4.4	2.4
J1612−5022	2012-07-24-09:40:05/05	12.0	–	0.23(3)	15.2	50.4	7.2	3.7
J1615−4958	2012-07-24-09:40:05/11	14.2	<7.7	0.158(17)	9.13	61.8	4.3	2.4
J1618−4624	2012-04-01-13:59:20/07	15.1	7.8	0.273(13)	0.291	1.02	1.5	2.5
J1634−4229	2012-03-31-19:56:13/07	19.9	–	0.16(2)	15.0	82.2	7.3	57.5
J1653−4105	2012-09-24-04:17:22/12	15.8	8.8	0.269(16)	22.8	45.0	9.3	53.0
J1653−45	2012-07-20-11:04:49/02	11.2	–	–	15.9	29.1	–	–
J1704−3756	2011-12-23-20:33:36/05	11.3	–	0.134(15)	11.7	21.3	4.7	31.1
J1706−4434	2011-12-12-05:16:53/05	16.9	–	0.19(2)	11.8	21.6	14.5	70.9
J1719−3458	2012-04-13-15:31:21/01	13.7	10.2	0.20(2)	21.0	25.9	10.2	53.3
J1727−2951	2011-10-12-03:10:49/04	16.7	–	0.514(8)	11.4	18.9	7.6	15.1
J1731−33	2012-10-04-10:29:13/13	11.6	–	–	48.4	88.7	–	–
J1734−2859	2011-12-07-03:42:23/10	10.4	6.6	0.13(2)	8.72	26.5	3.2	17.1
J1745−23	2012-12-09-23:10:30/01	14.3	–	–	0.660	1.22	–	–
J1749−2146	2012-04-01-17:39:19/07	16.9	10.8	–	121.3	153.2	–	–
J1753−28	2013-02-01-01:43:53/09	19.8	8.2	–	3.90	7.85	–	–
J1757−1854	2012-04-12-16:27:35/03	13.3	–	0.25(4)	0.705	1.80	13.7	96.0
J1810−1709	2011-12-31-22:59:57/05	13.9	–	0.45(4)	134.2	309.0	38.3	94.7
J1812−15	2011-10-11-06:44:35/06	42.5	–	–	18.7	34.2	–	–
J1812−20	2012-07-21-15:18:42/08	23.2	10.7	–	102.8	392.0	–	–
J1822−0719	2012-08-03-11:58:41/07	11.4	–	–	10.1	18.5	–	–
J1822−0902	2012-04-02-18:07:28/13	16.5	12.4	–	5.25	7.11	–	–
J1831−04	2011-12-28-01:09:49/03	18.4	–	–	15.3	28.1	–	–
J1835−0600	2011-10-11-07:58:09/13	16.2	8.6	–	29.0	53.6	–	–
J1851−06[a]	2012-08-04-14:47:04/06	9.5	<6.6	–	50.2	63.9	–	–
J1854−0524	2012-04-11-21:49:28/01	23.0	–	–	12.6	23.3	–	–

Note. [a]PSR J1851−06 was later discovered independently during the commissioning of FAST and its pilot observations for the Commensal Radio Astronomy FAST Survey (CRAFTS; Li et al. 2018).

indicates a successful application of the segmented-search strategy to a relativistic binary pulsar.

4 NEWLY DISCOVERED PULSARS

A total of 40 new pulsars[10] have been discovered in data processed for this paper (see Table 2). All but one of these pulsars have been successfully confirmed through reobservation with the Parkes 64-m Radio Telescope using the gridding strategy outlined in Section 2.1. The remaining pulsar (PSR J1831−04) displays evidence of nulling and/or intermittency in its discovery observation (see Section 5.7) and is considered sufficiently unambiguous in this observation so as to be 'self-confirmed'.[10]

As of the time of writing, 7 of the 40 newly discovered pulsars lack sufficient pulse times-of-arrival (TOAs) for the determination of unique phase-connected timing solutions. These pulsars have been allocated temporary names listing only two digits of declination

[10]A candidate can be considered *'self-confirmed'* if it is detected with a high S/N (e.g. >15), exhibits broadband and continuous emission, and has a DM constrained away from 0 cm^{-3} pc, such that the likelihood of it not representing a genuine pulsar detection is remote.

Table 3. Discovery parameters of the seven newly discovered pulsars for which full timing solutions are not yet available. The reported spin period (P) and dispersion measure (DM) of each pulsar is taken from its discovery observation. The reported position of each pulsar in both equatorial (RA and Dec.) and Galactic (l and b) coordinates represents the best-known gridded position of the pulsar following confirmation observations. DM distances are calculated according to the NE2001 model (left column; Cordes & Lazio 2002) and the YMW16 model (right column; Yao et al. 2017). Values in parentheses represent 1σ uncertainties on the final digit.

PSR name	RA (J2000) (hms)	Dec. (J2000) (°′″)	l (°)	b (°)	P (ms)	DM (cm^{-3} pc)	Dist. (kpc)	
J1653−45[a]	16:53.9(3)	−45:17(7)	340.75	−0.97	950.977(3)	207(9)	3.6	3.5
J1731−33	17:31.8(4)	−33:48(7)	354.31	−0.11	606.9003(16)	571(9)	6.1	4.3
J1745−23[a]	17:45.5(4)	−23:25(7)	4.70	2.89	5.416 699 86(14)	244.94(9)	4.5	7.9
J1753−28	17:53.1(4)	−28:53(7)	0.89	−1.38	85.858 61(2)	18.0(9)	0.6	0.7
J1812−15[a]	18:12.6(5)	−15:31(7)	14.74	1.29	1014.529(3)	431(10)	5.9	10.0
J1831−04[b]	18:31.0(5)	−04:29(7)	26.62	2.49	1065.578(3)	216(10)	4.4	4.9
J1851−06	18:51.2(5)	−06:38(7)	27.08	−3.02	1920.312(13)	220(20)	4.8	5.7

Notes. [a]Indicates confirmed binary pulsars.
[b]Indicates candidate binary pulsars.

Table 4. Best-fitting TEMPO2 timing parameters for 28 pulsars, including their positions in both equatorial (RA and Dec.) and Galactic (l and b) coordinates, spin periods (P), spin-period derivatives ($\dot{P}$), and dispersion measures (DM). Values in parentheses represent 1σ uncertainties on the final digit. DM distances are calculated according to the NE2001 model (left column; Cordes & Lazio 2002) and the YMW16 model (right column; Yao et al. 2017).

PSR name	RA (J2000) (hms)	Dec. (J2000) (°′″)	l (°)	b (°)	P (ms)	$\dot{P}$ (10^{-18})	DM (cm^{-3} pc)	Dist. (kpc)	
J1136−6527	11:36:25.22(7)	−65:27:19.5(3)	295.24	−3.71	1189.30900495(8)	1750(16)	164.1(18)	3.4	2.0
J1210−6322	12:10:46.78(10)	−63:22:20.9(6)	298.40	−0.86	1163.18571439(18)	9247(12)	547(5)	10.9	9.6
J1223−5856	12:23:40.14(3)	−58:56:48.9(2)	229.35	3.73	288.54142685(2)	5.7(8)	233(3)	5.3	4.8
J1300−6602	13:00:26.93(3)	−66:02:16.8(2)	303.85	−3.18	1143.31584211(4)	335(2)	460(3)	13.4	15.6
J1344−5855	13:44:53.05(3)	−58:55:24.77(18)	309.79	3.23	252.397929468(5)	2914.5(17)	294.1(6)	6.5	7.5
J1430−5712	14:30:16.17(2)	−57:12:31.4(2)	316.04	3.13	491.518803580(9)	46940.8(16)	149(4)	3.0	3.9
J1434−5943	14:34:58.31(2)	−59:43:41.6(2)	315.65	0.56	1072.12121207(3)	29.6(18)	126(3)	2.4	3.2
J1504−5659	15:04:31.987(17)	−56:59:19.4(2)	320.33	1.32	1672.37234272(3)	1428(3)	454.2(11)	7.3	11.3
J1507−5800	15:07:03.504(8)	−58:00:56.20(10)	320.12	0.26	897.254102404(11)	260.3(6)	429.5(5)	6.1	5.9
J1513−6013	15:13:54.02(4)	−60:13:26.5(3)	319.75	−2.09	1958.73704232(12)	1371(8)	322.7(16)	5.7	7.9
J1514−5316	15:14:40.160(11)	−53:16:02.3(2)	323.46	3.80	296.279212139(4)	1.6(5)	27.1(3)	0.9	0.9
J1557−5151	15:57:29.30(2)	−51:51:08.4(3)	329.56	1.13	408.154708451(8)	75.4(9)	464(3)	8.7	6.5
J1603−5312	16:03:50.88(3)	−53:12:58.0(4)	329.40	−0.53	839.22081265(6)	49600(5)	142(3)	4.2	3.1
J1612−5022	16:12:28.028(12)	−50:22:57.3(4)	332.30	0.66	1368.28292337(6)	34(4)	248.7(15)	5.5	4.0
J1615−4958	16:15:17.38(3)	−49:58:02.0(4)	332.91	0.65	558.25750561(3)	1461(8)	240.7(6)	5.2	3.9
J1634−4229	16:34:14.665(9)	−42:29:44.3(4)	340.54	3.54	2015.26299651(4)	8010(2)	337.9(10)	6.7	18.9
J1653−4105	16:53:25.374(10)	−41:05:25.6(4)	343.95	1.76	498.978065960(7)	54.1(11)	419.4(12)	5.9	14.0
J1704−3756	17:04:57.466(15)	−37:56:42.9(8)	347.80	1.95	305.234449799(11)	11284(3)	405.7(6)	5.9	15.2
J1706−4434	17:06:23.183(9)	−44:34:30.0(2)	342.67	−2.26	429.922423250(6)	2578(2)	467.0(6)	8.8	19.4
J1719−3458	17:19:12.141(3)	−34:58:22.4(2)	351.89	1.39	493.774733755(3)	14.9(3)	530.0(3)	7.2	16.4
J1734−2859	17:34:00.114(10)	−28:59:53.4(16)	358.60	2.12	301.455877926(9)	8.0(6)	313.9(9)	4.9	11.4
J1749−2146	17:49:21.241(19)	−21:46:31(10)	6.57	2.98	2714.55556146(12)	7077(7)	260(20)	4.8	9.6
J1810−1709	18:10:28.21(3)	−17:09:27(4)	13.05	0.96	1161.13257983(7)	333(6)	670(20)	9.3	14.6
J1812−20	18:12:36.58(5)	−20:58.1(5)	9.95	−1.32	1903.1119816(5)	240(30)	457(19)	6.7	11.3
J1822−0719	18:22:28.073(15)	−07:19:55.0(7)	23.10	3.04	499.07553362(4)	19(2)	199(5)	4.2	4.6
J1822−0902	18:22:35.745(8)	−09:02:59.1(5)	21.59	2.21	148.894507003(3)	17780.9(8)	448.1(15)	7.9	15.7
J1835−0600	18:35:20.25(5)	−06:00:00(4)	25.76	0.83	2221.7871479(14)	8430(80)	780(20)	9.8	10.6
J1854−0524	18:54:55.35(2)	−05:24:23.1(19)	28.51	−3.24	544.02080981(15)	1200(10)	192(3)	4.5	5.0

and are listed in Table 3. The remaining 33 pulsars for which full timing solutions have been developed are listed in Tables 4, 5, and 6 (with the exception of PSR J1757−1854). Pulsars in these tables for which the uncertainty in declination is greater than or equal to 0.5 arcmin have also been assigned a temporary name with only two digits of declination.

Timing observations for each pulsar were conducted by the Parkes 64-m Radio Telescope and the Jodrell Bank 76-m Lovell Radio Telescope. At Parkes observations were conducted with an approximately monthly cadence. Jodrell Bank timing observations were conducted with an irregular cadence, with observations made of each pulsar typically every 1–3 weeks. Parkes observations were conducted using two receivers, the MB20 receiver and the H-OH 21-cm receiver.[11] The two timing backends employed at Parkes include a Digital Filter Bank backend system (DFB4), capable only

[11]The H-OH receiver was used between MJD 57440 and 57727 due to the unavailability of the MB20 receiver.

Table 5. Fit-related timing parameters for 28 pulsars, including the data span, the period reference epoch, the number of TOAs used to derive each timing solution as listed in Table 4, the root mean square (RMS) of the weighted TEMPO2 fit and the unweighted reduced χ^2 ($\chi^2_{\rm red}$). Derived parameters, including the characteristic age ($\tau_{\rm c}$), the surface magnetic field ($B_{\rm surf}$) and the spin-down luminosity ($\dot{E}$) are calculated according to the equations presented in Lorimer & Kramer (2005) and are given to a precision consistent with the measurements of P and $\dot{P}$ used to derive them, up to a maximum of three significant figures.

PSR name	Data span (MJD)	Epoch (MJD)	$n_{\rm TOA}$	RMS (μs)	$\chi^2_{\rm red}$	$\tau_{\rm c}$ (Myr)	$B_{\rm surf}$ (10^{10} G)	$\dot{E}$ (10^{30} erg s^{-1})
J1136−6527	57732−58152	57895	28	1559	1.2	10.7	144	41.1
J1210−6322	57530−58057	57648	38	4693	1.4	1.99	328	232
J1223−5856	57372−58058	57405	46	2074	1.4	800	4.1	9
J1300−6602	57372−58128	57554	46	1659	0.7	53.9	61.9	8.85
J1344−5855	57732−58152	57942	43	1152	1.4	1.37	85.8	7160
J1430−5712	57324−57845	57562	28	984	1.0	0.165	480	15600
J1434−5943	57296−58058	57530	54	1628	1.6	570	17.8	0.95
J1504−5659	57229−57845	57483	35	1172	1.7	18.5	155	12.1
J1507−5800	57442−58127	57604	40	502	0.9	54.5	48.3	14.2
J1513−6013	57500−58057	57633	55	2549	1.4	22.6	164	7.21
J1514−5316	57837−58337	57892	46	561	1.8	2900	2.2	2
J1557−5151	57066−57845	57359	36	1488	0.6	85.5	17.5	43.8
J1603−5312	57586−58057	57693	48	1819	1.0	0.267	645	3310
J1612−5022	57837−58337	57947	50	1116	0.9	640	21.6	0.52
J1615−4958	57798−58128	57928	33	653	0.9	6.04	90.3	332
J1634−4229	57442−58128	57603	27	656	0.5	3.98	402	38.7
J1653−4105	57613−58153	57883	66	1484	1.0	146	16.4	17.2
J1704−3756	57500−57866	57650	33	822	1.0	0.427	186	15700
J1706−4434	57231−58126	57416	57	653	1.3	2.63	105	1280
J1719−3458	57473−58059	57637	55	421	1.1	520	8.58	4.9
J1734−2859	57500−58117	57674	27	673	0.9	600	4.91	12
J1749−2146	57513−58115	57656	19	1213	1.1	6.06	438	14.0
J1810−1709	57357−58123	57573	26	2612	1.3	55	62.2	8.4
J1812−20	57512−58077	57615	27	3976	0.6	130	68	1.4
J1822−0719	57657−58137	57700	21	836	1.5	420	9.7	6.0
J1822−0902	57420−58116	57566	49	952	84.7	0.132	163	213000
J1835−0600	57716−58126	57733	18	1714	1.2	4.16	433	30.4
J1854−0524	57714−58149	57737	48	2288	13.2	7.16	80.8	294

of incoherent dedispersion, and the CASPER Parkes Swinburne Recorder[12] (CASPSR), capable of coherent dedispersion. Additionally, search-mode filterbank data taken using the Berkeley Parkes Swinburne Recorder[13] (BPSR) to HTRU specifications (see Keith et al. 2010) was also used in the early timing stages of multiple pulsars. Jodrell Bank observations were conducted using the single-pixel *L*-band receiver in combination with both a DFB backend and an ROACH[14] backend (Bassa et al. 2016) capable of coherent dedispersion. A summary of the receivers and backends used in this project[15] is presented in Table 7.

Each timing solution was determined using multiple software packages including the DSPSR[16] (van Straten & Bailes 2011), PSRCHIVE[17] (Hotan, van Straten & Manchester 2004), SIGPROC[18] (Lorimer 2011), and PRESTO[19] (Ransom 2001) pulsar data analysis packages as well as the TEMPO[20] and TEMPO2[21] (Hobbs, Edwards & Manchester 2006) timing software packages. Each observation was first cleaned to remove instances of time and frequency-domain RFI, and then calibrated against an observation of a pulsed noise diode to account for the differential gain and phase between the receiver's polarization feeds. TOAs were then produced by summing each observation in both frequency and polarization, before partially summing in time and cross-correlating each summed profile against a standard reference pulse profile. Initial timing solutions were typically developed using the TEMPO software package, often with the use of a modified prototype version of the DRACULA[22] software package, which solves for the global rotation count of a pulsar between discrete observations using the phase-jump technique described by Freire & Ridolfi (2018). The finalized timing solutions presented in Tables 4 and 5 were produced using TEMPO2, after first reweighting each set of TOAs such that their reduced $\chi^2 = 1$. All solutions in Tables 4 and 5 are in TCB[23] units and use the DE421[24] planetary ephemeris.

[12] http://www.astronomy.swin.edu.au/pulsar/?topic = caspsr
[13] http://www.astronomy.swin.edu.au/pulsar/?topic = bpsr
[14] Based on the ROACH FPGA processing board, see https://casper.berkeley.edu/wiki/ROACH
[15] For the timing specifications of PSR J1757−1854, refer to Cameron et al. (2018).
[16] https://sourceforge.net/projects/dspsr
[17] http://psrchive.sourceforge.net
[18] http://sigproc.sourceforge.net
[19] http://www.cv.nrao.edu/ sransom/presto
[20] http://tempo.sourceforge.net
[21] http://www.atnf.csiro.au/research/pulsar/tempo2
[22] https://github.com/pfreire163/Dracula
[23] Barycentric Coordinate Time.
[24] https://ssd.jpl.nasa.gov/?ephemerides#planets

Table 6. Best-fitting TEMPO2 timing parameters for four newly discovered binary pulsars. Values in parentheses represent 1σ uncertainties on the final digit. Values quoted as upper limits represent an uncertainty of 3σ. DM distances are calculated according to the NE2001 model (Cordes & Lazio 2002) and the YMW16 model (Yao et al. 2017).

Parameter	J1537−5312	J1547−5709	J1618−4624	J1727−2951
Right ascension, α (J2000)	15:37:37.69466(18)	15:47:24.1248(12)	16:18:52.77579(13)	17:27:00.402(5)
Declination, δ (J2000)	−53:12:25.057(3)	−57:09:17.5699(16)	−46:24:34.950(4)	−29:51:40.8(8)
Spin period, P (ms)	6.927 095 508 3835(15)	4.291 146 064 1714(6)	5.931 367 495 2810(16)	28.404 953 4402(6)
Spin period derivative, $\dot{P}$ (10^{-18})	0.015 86(11)	0.007 45(3)	0.003 10(10)	0.31(6)
Dispersion measure, DM ($\mathrm{cm^{-3}\,pc}$)	117.52(5)	95.727(8)	125.364(16)	215.1(3)
Binary model	ELL1	ELL1	ELL1	ELL1
Orbital period, P_b (d)	3.550 148 38(2)	3.077 476 982(5)	1.780 433 535(2)	0.395 1890(4)
Projected semimajor axis, x (lt-s)	1.982 433(4)	2.668 161(2)	5.329 375(4)	0.057 83(11)
Epoch of the ascending node, T_asc (MJD)	57 295.061 729(3)	57 297.585 0363(6)	57560.5896560(4)	57845.1434(2)
$\lvert e\sin\omega\rvert$, $\lvert\epsilon_1\rvert$ (10^{-4})	<0.149	<0.0576	<0.0444	<130
$\lvert e\cos\omega\rvert$, $\lvert\epsilon_2\rvert$ (10^{-4})	<0.107	<0.0431	<0.0355	<147
Inferred eccentricity, e (10^{-6})	<11.9	<4.75	<4.27	<14200
Mass function, f ($10^{-3}\,\mathrm{M_\odot}$)	0.663 721(4)	2.153 422(5)	51.26961(11)	0.001330(7)
Minimum companion mass[a], $m_\mathrm{c,min}$ ($\mathrm{M_\odot}$)	0.115 0667(2)	0.174 793 58(15)	0.587 1916(5)	0.013 85(2)
Median companion mass[b], $m_\mathrm{c,med}$ ($\mathrm{M_\odot}$)	0.133 9705(3)	0.204 351 98(17)	0.704 4464(6)	0.016 01(3)
First TOA (MJD)	57 259	57 091	57 404	57 839
Last TOA (MJD)	58 136	58 136	58 136	58 299
Timing epoch (MJD)	57 575	57 445	57 637	57 958
Number of TOAs, n_TOA	92	90	98	106
Weighted RMS residuals (μs)	21	11	18	755
Reduced χ^2	0.8	1.4	0.8	1.0
Galactic longitude, l (°)	326.35	325.08	335.82	357.04
Galactic latitude, b (°)	1.94	−2.05	2.79	2.92
DM distance, d (kpc)				
NE2001	2.9	1.9	2.4	3.8
YMW16	3.1	2.7	3.0	5.4
Characteristic age, τ_c (Myr)	6900	9100	30 200	1400
Surface magnetic field, B_surf (10^{10} G)	0.0331	0.0179	0.0136	0.30
Spin-down luminosity, $\dot{E}$ ($10^{30}\,\mathrm{erg\,s^{-1}}$)	1880	3700	590	500

Notes. [a]$m_\mathrm{c,min}$ is calculated for an orbital inclination of $i = 90°$ and an assumed pulsar mass of $1.4\,\mathrm{M_\odot}$.
[b]$m_\mathrm{c,med}$ is calculated for an orbital inclination of $i = 60°$ and an assumed pulsar mass of $1.4\,\mathrm{M_\odot}$.

Table 7. Specifications of the telescope receiver and backend combinations used for timing observations, including the antenna gain (G), system temperature (T_sys), central observing frequency (f_c), and observing bandwidth (B).

Telescope	Receiver	G ($\mathrm{K\,Jy^{-1}}$)	T_sys (K)	Backend	f_c (MHz)	B (MHz)
Parkes	MB20	0.74	23	BPSR[a]	1382	400
				DFB4	1369	256
				CASPSR[a]	1382	400
	H-OH	0.83	25	DFB4	1369	256
				CASPSR[a]	1382	400
Jodrell	*L*-band	1.00	28	DFB	1532	384
				ROACH	1527	400

Note. [a]The usable bandwidth of BPSR and CASPSR is reduced to 340 MHz due to the presence of strong RFI from the *Thuraya 3* satellite and an associated RF filter.

For the 27 pulsars observed using the Parkes DFB4 backend and with full phase-connected timing solutions, it is also possible to determine calibrated 1.4-GHz flux densities (S_{1400}). Following polarization calibration, each observation was flux calibrated against an observation of Hydra A,[25] which was typically separated in time from the pulsar observation by as much as 1–2 weeks. The phase-connected timing solution of each pulsar was then used to sum together the DFB4 observations so as to produce an integrated observation from which a measurement of flux density was derived. However, as the observed position of the pulsar is typically offset from the final timed position of the pulsar, an additional flux-density correction based on the offset in position (θ) was applied using equation (5). The resulting values of S_{1400} are listed in Table 2. Also derived are the 1.4-GHz luminosities of each pulsar, $L_{1400} = S_{1400} \times d^2$, where d is the distance of each pulsar in kpc. Using the DM of each pulsar, a DM distance d can be estimated based upon two separate models of the Galactic distribution of electron density, the NE2001 model (Cordes & Lazio 2002) and the YMW16 model (Yao et al. 2017). These distance estimates are listed both in Tables 3 and 4, while the corresponding values of L_{1400} are listed in Table 2.

Fig. 2 shows the integrated 1.4-GHz pulse profiles for each of the newly discovered pulsars, folded with 256 phase bins. In the case of the 27 pulsars timed using Parkes and with full phase-connected timing solutions, each integrated profile was produced by coherently summing the pulsar's timing observations. The integrated profiles of PSRs J1537−5312, J1547−5709, J1618−4624, J1727−2951, and J1757−1854 (for which the intrachannel dispersion smearing of DFB4 becomes a significant factor) were produced using coherently dedispersed CASPSR data, while the remaining 22 pulse profiles were produced from DFB4 data. Profiles for the 13 pulsars without

[25]Recorded as part of the Parkes Pulsar Timing Array (PPTA) project (see e.g. Yan et al. 2011).

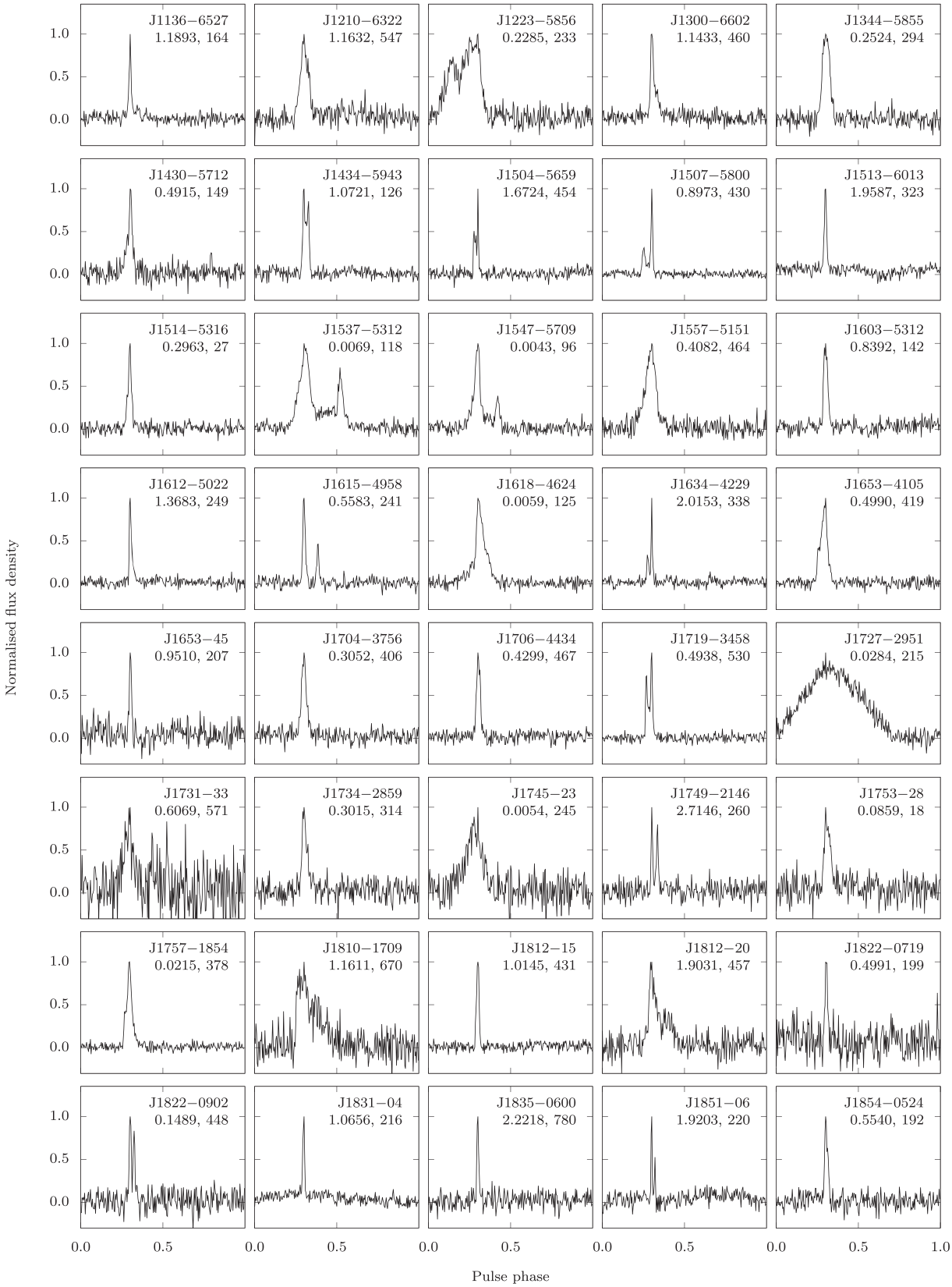

Figure 2. Integrated pulse profiles of the 40 newly discovered pulsars. Each profile consists of 256 phase bins, has had its peak amplitude normalized to unity and has been rotated such that its peak is at a pulse phase of 0.3. Listed in the top right of each profile is the pulsar's current name, spin period (s) and DM (cm^{-3} pc).

Parkes data or without phase-connected timing solutions were produced using either their discovery HTRU observation or their subsequent confirmation observation, whichever resulted in a higher value of S/N. All pulse profiles have had their baselines subtracted and peak amplitudes normalized to unity, and have been rotated such that the profile peak is located at a pulse phase of 0.3. For each integrated profile, an analytic model profile consisting of multiple Gaussian components was derived using the PSRCHIVE application PAAS and used to measure the pulse widths at 10 per cent (W_{10}) and 50 per cent (W_{50}) of the profile peak. These pulse widths are listed in Table 2.

Of the 40 newly discovered pulsars reported in this paper, 8 have been conclusively determined to be in binary systems. The phase-connected timing solutions of four of these pulsars (PSRs J1537−5312, J1547−5709, J1618−4624, and J1727−2951) are presented in Table 6, while the solution and properties of PSR J1757−1854 have been previously published in Cameron et al. (2018). The remaining three confirmed binary pulsars (PSRs J1653−45, J1745−23, and J1812−15) are highlighted in Table 3. An additional pulsar also displays evidence which strongly suggests that it also represents a new binary system; this pulsar (PSR J1831−04) is also presented in Table 3. All of these binary systems are discussed in detail in Section 5.

4.1 Redetections in the PMPS

The HTRU-S LowLat survey area has a complete overlap with the survey area of the PMPS. A comprehensive search of PMPS archival data was therefore carried out to determine if any of the newly discovered pulsars reported in this paper was detectable in the earlier survey. All PMPS beams within one beamwidth (∼0.24°) of the best known position of each pulsar were searched for matching pulsar candidates. For those pulsars with full timing solutions, a direct ephemeris fold of each observation was also produced and inspected. For those pulsars for which a detection was made, the maximum S/N derived from all inspected PMPS beams (S/N_{PMPS}) is recorded in Table 2.

In total, 22 pulsars were detected in the archival PMPS data. Of these, 13 were detected above the theoretical S/N cutoff for pulsars in the PMPS, $S/N_{min,PMPS} = 8$ (Manchester et al. 2001). Therefore, these pulsars were theoretically detectable in the earlier survey, but for reasons unknown were overlooked, potentially as a result of the large number of pulsar candidates produced during the processing of the PMPS or due to the presence of RFI. It should be noted that many of the pulsars detected in the PMPS using an ephemeris fold were not detected by a simple application of standard searching techniques (e.g. an FFT-based search). This difficulty in detection might also partially account for the previous non-discovery of these pulsars, and may allow for further PMPS detections in the future as additional timing solutions are derived. The remaining nine pulsars were detected only weakly in the PMPS, falling below the $S/N_{min,PMPS}$ cut-off. In cases where the PMPS detection is only tentative, the measured S/N_{PMPS} is set as an upper limit.

4.2 Gamma-ray and supernova remnant associations

We note at the outset that the chances of determining an association between any of the newly discovered pulsars and a supernova remnant (SNR) would appear to be unlikely. SNRs have typical lifetimes of only 10^4 yr (Frail, Goss & Whiteoak 1994), while the youngest pulsars among our discoveries have characteristic ages of the order of 10^5 yr. While an SNR association is not impossible for pulsars in this age range, the lack of a well-measured proper motion for any of the discovered pulsars makes confirming any such association (should it exist) all the more difficult.

Nevertheless, we have attempted to evaluate the possibility of an SNR association for the four youngest pulsars (PSRs J1430−5712, J1603−5312, J1704−3756, and J1822−0902), each of which has a characteristic age $\tau_c < 1$ Myr. A radius of association (r_A) was determined for each pulsar by taking the distribution of pulsars (as listed by PSRCAT) with constrained proper motions and $\tau_c < 1$ Myr. Using DM-distance estimates from both the NE2001 and YMW16 models, these proper motions were then converted into tangential velocities (V_T), of which the median value was taken. Using the characteristic age and DM-distance estimates of each of the newly discovered pulsars (as listed in Tables 4 and 5), these median V_T values were converted into angular offsets, of which the larger was taken as r_A. The pulsars were then cross-matched against the Green SNR Catalogue[26] (Green 2019) for SNRs falling within these radii.

For PSRs J1430−5712, J1704−3756, and J1822−0902 (with r_A values of 0.89°, 1.17°, and 0.27°, respectively), no SNR were identified. However, as these systems may have higher proper motions than assumed in our calculations, an undetected SNR association cannot be ruled out. Meanwhile, PSR J1603−5312 (with an r_A of 1.29°) was found to coincide with two SNR, namely G328.4+00.2 and G329.7+00.4 (separated by 1.25° and 0.99°, respectively). In the case of G328.4+00.2, an association with PSR J1603−5312 seems unlikely, as Gelfand et al. (2007) argue an age for the SNR of only ∼ 6500 yr, approximately 40 times smaller than the pulsar's characteristic age. Furthermore, they argue that G328.4+00.2 is in fact a pulsar wind nebula (PWN) with its own embedded, as-yet undetected NS. In short, these facts would rule out any association between G328.4+00.2 and PSR J1603−5312. No age has been determined for G329.7+00.4, and at present an association with PSR J1603−5312 can be neither confirmed nor ruled out.

We have also not identified any gamma-ray associations for any of the newly discovered HTRU-S LowLat pulsars. This was determined by conducting a search of ∼ 9.6 yr of data recorded by the Large Area Telescope (LAT) on the *Fermi Gamma-Ray Space Telescope*. For each of the 33 pulsars with a phase-connected timing solution, a search was conducted using its best ephemeris, with details presented in Smith et al. (2019). The lack of gamma-ray detections is not surprising, given that only one of the newly discovered pulsars (PSR J1430−5712) has an $\sqrt{\dot{E}}/d^2 > 10^{16}\ \left(\mathrm{erg\,s^{-1}}\right)^{1/2}\ \mathrm{kpc^{-2}}$, a typical criterion for gamma-ray pulsars (Abdo et al. 2013). With additional timing, it is possible that the remaining unsolved pulsars may be shown to be associated with gamma-ray sources.

5 INDIVIDUAL PULSARS OF INTEREST

In addition to the previously published PSR J1757−1854, several of the pulsars discovered as part of this work warrant additional scientific scrutiny. They are discussed in the subsections below.

[26] http://www.mrao.cam.ac.uk/surveys/snrs/ (2019 June version).

5.1 PSR J1537–5312 and PSR J1547–5709, a pair of He-WD binary MSPs

PSRs J1537−5312 and J1547−5709 are a pair of binary MSPs whose parameters are listed in Table 6. Based on their respective spin periods of 6.93 and 4.29 ms as well as their low spin-period derivatives ($\sim 10^{-20}$ to 10^{-21}), both of these pulsars appear to be highly recycled. The highly circularized orbits and the range of companion masses implied by their mass functions (with minimum masses of $m_c = 0.115\,M_\odot$ and $m_c = 0.175\,M_\odot$, respectively) suggest that each pulsar possesses a degenerate helium white dwarf (He-WD) companion. These systems most-likely formed out of low-mass X-ray binaries (LMXB) through Case B Roche lobe overflow (RLO) (see e.g. Tauris 2011). No known counterpart to these companion WDs can be found in the SIMBAD astronomical database[27] (SIMBAD; Wenger et al. 2000) to within a radius of 30 arcsec, and no further confirmation observations of the WDs have been attempted. Such identifications may prove difficult given the large estimated distance to both pulsars ($\sim$ 2–3 kpc) along with their positions in the interstellar medium-dense Galactic plane.

Work conducted over several decades (e.g. Tauris & Savonije 1999; Tauris & van den Heuvel 2014) has implied the existence of a significant correlation between P_b and m_c for He-WD binaries, which is independent of the original low-mass progenitor star of the WD. With reference to equation 20 of Tauris & Savonije (1999), this correlation can be used to estimate the mass of the He-WD companions of both pulsars, although this estimate should be treated with a degree of caution given the limited information available. Taking an average between the Pop. I and Pop. II cases outlined in Tauris & Savonije (1999), the estimated He-WD masses are $m_{c,calc} \simeq 0.23\,M_\odot$ in the case of both pulsars.

Using these calculated WD masses (and assuming the mass of each pulsar), we can in turn estimate the inclination angles of the orbits of PSRs J1537−5312 and J1547−5709 (with reference to equation 4). Assuming a canonical pulsar mass of $m_p = 1.4\,M_\odot$ gives an inclination angle $i \simeq 32^\circ$ for PSR J1537−5312 and $i \simeq 53^\circ$ for PSR J1547−5709. Varying the pulsar mass between 1.3 and 2.0 $M_\odot$ allows the inclination angle to vary between $i = 30^\circ$ and 41° for PSR J1537−5312 and between $i = 49^\circ$ and 78° for PSR J1547−5709. Naturally, the true value of i in each case is highly dependent on the true mass of the pulsar, but it would appear from this analysis that the orbit of PSR J1537−5312 is unlikely to be highly inclined, while the orbit of PSR J1547−5709 may possess a high inclination should the pulsar be among the most massive of those currently known. A future detection of Shapiro delay in either pulsar would be able to provide an observational handle on the inclination angles and masses of both the pulsar and its He-WD companion, but such a detection will require more sensitive observations than are currently available from Parkes.

5.2 PSR J1618–4624, an unusual CO-WD binary MSP

At first glance the 5.93-ms pulsar PSR J1618−4624 appears similar to PSRs J1537−5312 and J1547−5709, as it is also a highly recycled MSP in a circular orbit around a probable WD companion (see Table 6). However, with a minimum mass of $m_c = 0.587\,M_\odot$, PSR J1618−4624's companion is most likely a carbon–oxygen white dwarf (CO-WD), representing a much rarer class of MSP-WD binary which likely evolved from an intermediate-mass X-ray binary (IMXB) (Tauris 2011). Only a handful of these systems are known to exist, including PSR J1614−2230 (Demorest et al. 2010; Lin et al. 2011; Tauris, Langer & Kramer 2011; Tauris, Langer & Kramer 2012), PSR J1101−6424 (Ng et al. 2015) and recently PSR J1933−6211 (Graikou et al. 2017). No known counterpart to the CO-WD companion can be found in SIMBAD to within a radius of 30 arcsec, and no further confirmation observations have been attempted.

PSR J1618−4624 further stands out as a result of the unusual puzzle presented by the scenario of its formation and evolution. As described in Tauris (2011), the fully recycled nature of this pulsar combined with a CO-WD companion favours a formation scenario involving Case A RLO, in which a long and stable mass transfer occurs while the donor companion star is still on the main sequence (MS), thereby allowing the pulsar to fully spin-up. However, a Case A scenario can only account for the ∼1.78-d orbit of PSR J1618−4624 if the final mass of the neutron star is significantly lighter than the canonical value (see e.g. Tauris et al. 2011), with 'conventional' Case A RLO scenarios favouring orbits $P_b \gtrsim 3$ d (Tauris 2011). Alternatively, the loss of angular momentum required to produce such a short orbit could imply a common-envelope (CE) evolutionary stage, during which the accreting NS becomes enveloped within the expanded outer layers of the donor star, a Case C RLO scenario. However, a Case C scenario cannot easily account for the observed degree of recycling (Tauris 2011).

This apparent conflict between the Case A and Case C RLO scenarios could potentially be solved by an eventual mass measurement of PSR J1618−4624, which given the system's binary properties would most likely have to be derived from a measurement of the Shapiro delay. However, given the unknown inclination of the PSR J1618−4624, the prospects of such a measurement from future observations remain uncertain. Even in the case of a fully inclined orbit of $i = 90^\circ$, the expected magnitude of the Shapiro delay is comparable to the current timing RMS of $\sim 18\,\mu$s, with the individual TOA errors also being of a similar magnitude. More sensitive observations capable of reducing these effects will therefore be required to further investigate any potentially measurable Shapiro delay in this pulsar.

5.3 PSR J1745–23, a black widow pulsar

PSR J1745−23 is a 5.42-ms MSP in a black-widow class binary system. Follow-up observations with Parkes covering a 153-d span between MJD 57798 and MJD 57951 have allowed the determination of an approximate orbital solution which is sufficiently accurate so as to be useful as a folding model at all available epochs (see Table 8). The orbit appears to be highly circular, although in the absence of a phase-connected solution, we are presently unable to accurately constrain either the eccentricity e or the longitude of periastron ω. Therefore, these values are both fixed at 0 in our model. Assuming a canonical pulsar mass of $m_p = 1.4\,M_\odot$, PSR J1745−23 would appear to have a rather light companion, with a minimum companion mass of $m_{c,min} \simeq 0.027\,M_\odot$ and a median mass of $m_{c,med} \simeq 0.031\,M_\odot$.

PSR J1745−23 also appears to eclipse during superior conjunction. The duration of this eclipse is not yet precisely constrained, however a conservative upper limit of the eclipse duration is $T_{eclipse} < 58$ min, occurring between orbital phases of $0.14 < \varphi < 0.38$ (as specified by the model in Table 8).

We classify PSR J1745−23 as a black widow (BW) based upon its lightweight companion, the presence of eclipses and the short

[27] http://simbad.u-strasbg.fr/simbad/

Table 8. Approximate binary parameters for PSR J1745−23. Values in parentheses, where available, represent 1σ uncertainties on the final digit after weighting the TOAs such that $\chi^2 = 1$.

PSR name	J1745−23
Fitting program	TEMPO
Binary model	BT
Orbital period, P_b (d)	0.165562(10)
Projected semimajor axis, x (lt-s)	0.06247(6)
Eccentricity, e	0[a]
Longitude of periastron, ω (°)	0[a]
Epoch of periastron, T_0 (MJD)	57950.47559(3)
Mass function, f (10^{-6} $M_\odot$)	9.550(16)
Minimum companion mass[b], $m_{c,min}$ ($M_\odot$)	0.02689(2)
Median companion mass[b], $m_{c,med}$ ($M_\odot$)	0.03111(4)

Notes. [a]Values fixed at 0 due to lack of constraint and an evidently highly circular orbit.
[b]$m_{c,min}$, $m_{c,med}$ calculated per the assumptions in Table 6.

orbital period ($P_b < 24$ h) (see e.g. Roberts 2013). This may also be partly responsible for the difficulties that have been encountered while attempting to develop a phase-connected solution for this pulsar, a problem noted in other BW systems, e.g. PSR J2051−0827 (Lazaridis et al. 2011; Shaifullah et al. 2016). At present, although the companion can be identified as both lightweight and likely degenerate, any further classification remains uncertain. Ongoing observations will aim to establish a phase-coherent solution for this pulsar.

5.4 PSR J1727–2951, an intermediate-period, low-mass binary pulsar

As can be seen in Fig. 2, PSR J1727−2951 immediately stands out due to its unusually wide pulse profile. With $W_{50} = 11.4$ ms and $W_{10} = 18.9$ ms, PSR J1727−2951 shows emission across the majority of its 28.4-ms pulse profile. The measured $\dot{P} = 3.1(6) \times 10^{-19}$ indicates a partially recycled pulsar, which is consistent with its binary nature.

PSR J1727−2951 is in a near-circular ∼9.5-h orbit (Table 6). Based upon the system's mass function and an assumed pulsar mass of $m_p = 1.4\,M_\odot$, the minimum mass for the companion is only $m_c \simeq 0.014\,M_\odot$. Even taking an inclination angle $i = 26°$, which constitutes a 90 per cent upper limit on the mass of the companion (Lorimer & Kramer 2005), m_c only increases to $\sim 0.032\,M_\odot$, still well below a typical He-WD mass. The system would therefore appear to be superficially similar to the BW pulsar PSR J1745−23 (see Section 5.3), in both its companion mass and small projected semimajor axis. However, unlike a typical BW system, PSR J1727−2951 is neither fully recycled nor does it display any evidence of eclipses, despite observational coverage of its entire orbital period. Nor does the pulsar appear to show the timing irregularities often typical of BW systems.

The true nature of PSR J1727−2951 therefore remains puzzling. Should the orbit be inclined in such a way so as to prevent the observation of eclipses, a BW classification remains a possibility (Freire 2005), as in the case of PSR J2214+3000 (Ransom et al. 2011). An alternative (although not mutually exclusive) view comes from the example of PSR J1502−6752 (Keith et al. 2012), a pulsar with which PSR J1727−2951 shares very similar values of both P and $\dot{P}$. Keith et al. (2012) identify PSR J1502−6752 as a member of the 'very low mass binary pulsars' (VLMBPs), first described by Freire et al. (2003). It would appear that based on its low value of m_c, PSR J1727−2951 also falls into this category, and may help bridge the gap between PSR J1502−6752 and the rest of the VLMBP population.

5.5 PSR J1653–45, a binary system with a long orbital period

PSR J1653−45 is a 0.95-s pulsar in a ∼1.45-yr orbit around an unknown binary companion which appears to eclipse the pulsar. Changes in the apparent spin period of PSR J1653−45 can be seen in Fig. 3. The cyclic nature of the pulsar's apparent spin period is clear evidence of a binary system, while the apparently predictable spans of non-detections as a function of orbital phase lends strong evidence to the eclipsing-binary hypothesis. When detectable, the apparent spin-period of the pulsar increases almost linearly, at an average rate of $\dot{P} \simeq 4.2 \times 10^{-12}$. From the two orbits we have observed thus far, we estimate an orbital period of $P_b \simeq 528$ d.

Due to the fact that the pulsar has remained undetected during roughly half of its orbital period, it has so far been impossible to develop either an orbital solution or a phase-connected timing solution. The near-linearity of its changing apparent spin-period during each orbit suggests that the system has a significant eccentricity, and estimates of the projected semimajor axis (∼500–700 lt-s) indicate a companion mass of the order of a solar mass. Combined with the observed eclipses, we speculate that the companion of PSR J1653−45 may be an MS star. If this is the case, PSR J1653−45 may be similar to another pulsar discovered earlier in this survey, PSR J1759−24 (Ng et al. 2015), which is also considered likely to be in an eclipsing binary system with a long orbital period. Other potential examples of similar systems include PSR B1820−11, a ∼280-ms pulsar in an eccentric ∼1-yr orbit around a companion speculated to either be an MS companion (Phinney & Verbunt 1991) or a possible NS/WD companion (Thorsett & Chakrabarty 1999), and PSR B1259−63, a ∼48-ms pulsar in an eccentric ∼3.4-yr orbit around a $\sim 10\,M_\odot$ Be-star companion and which also experiences a ∼40-d eclipse (Johnston et al. 1992).

5.6 PSR J1706–4434, a glitching pulsar

Following a confirmation and gridding observation on MJD 57169, timing observations with an approximately monthly cadence between MJD 57231 and MJD 57588 (a span of 357 d) were sufficient to develop a fully phase-connected solution for PSR J1706−4434. However, all further timing observations (spanning MJD 57615 to MJD 58126) showed a clear deviation from this model, indicating a sudden decrease in the spin period of the pulsar. From this, it can be concluded that a glitch occurred in PSR J1706−4434 at some point between MJD 57588 and MJD 57615. The effect of this glitch on the timing residuals of PSR J1706−4432 is shown in Fig. 4.

Table 9 lists the parameters of the observed glitch in PSR J1706−4434. Due to the limited cadence of timing observations surrounding the glitch, the precise glitch epoch cannot be accurately determined. A glitch epoch of MJD 57601, the approximate mid-way point between the epochs of the neighbouring observations, has therefore been assumed. Similarly, no evidence of a post-glitch relaxation has been detected, likely also due to the limited observational cadence as well as the limited timing precision of this pulsar. In addition, the permanent change to the spin-frequency derivative $\dot{\nu}$ (and corresponding change in the spin-period derivative $\dot{P}$) remains poorly constrained. Therefore, we present only an upper limit on this value in Table 9, which represents an uncertainty of $3\,\sigma$.

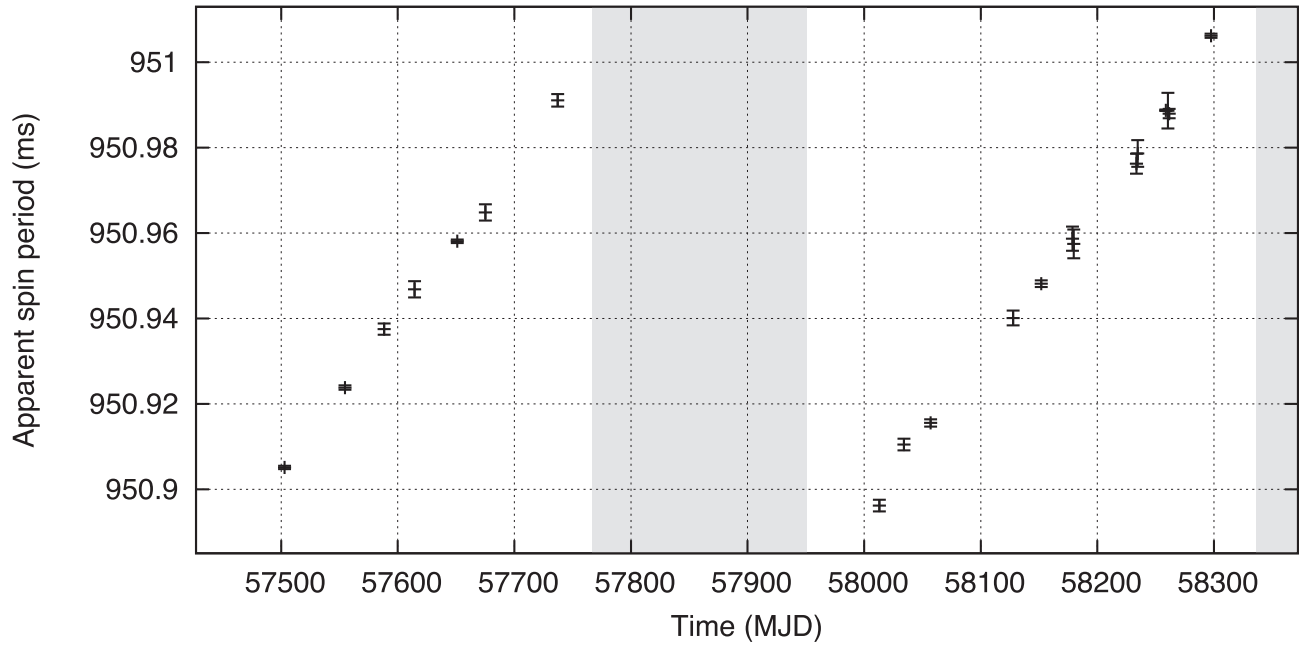

Figure 3. Changes in the apparent spin period of PSR J1653−45 over a span of approximately 2.2 yr. Error bars represent the 1σ error on the measured period at each epoch. Grey regions indicate spans of time during which the pulsar appeared to be undetectable.

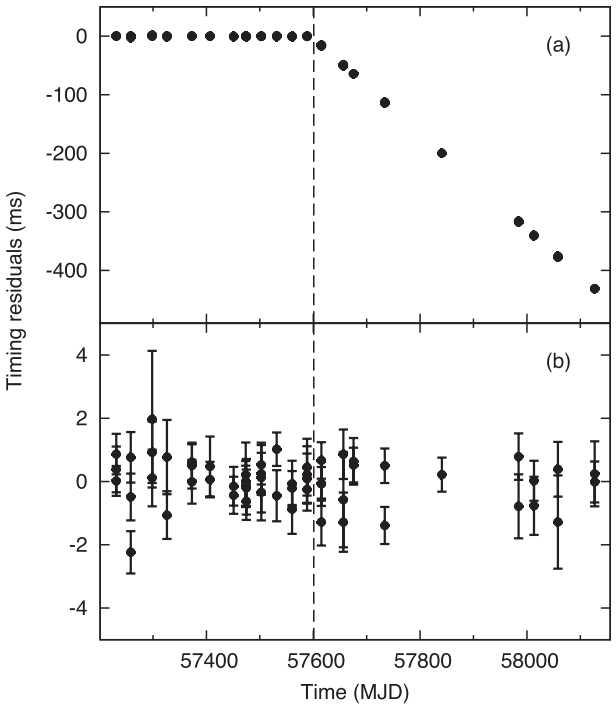

Figure 4. Effect of the glitch observed in PSR J1706−4434 on the pulsar's timing residuals. Plot (a) shows the residuals plotted using the best pre-glitch phase-connected solution for the pulsar, without accounting for the glitch. Plot (b) shows the residuals plotted using the final phase-connected solution, which incorporates the glitch parameters listed in Table 9. The glitch epoch (MJD 57601) is indicated by the dashed line.

5.7 PSR J1812–15 and PSR J1831–04, a pair of nulling, accelerated pulsars with long rotational periods

PSR J1812−15 and PSR J1831−04 have rotational periods of approximately 1014 and 1066 ms, respectively. Evidence for acceleration was found in the discovery observations of both pulsars [3.98(13) and 11.7(7) m s^{-2}, respectively], indicating that they are likely to be in binary systems. The case for the binary nature of PSR J1812−15 has been bolstered by a number of subsequent observations, during which its acceleration has been seen to vary between 3.62(11) and 5.57(9) m s^{-2} and its period between 1014.137(7) and 1014.931 02(16) ms, such that its binary nature is considered to be confirmed, although a complete orbital solution is currently unavailable. Meanwhile, despite a total of $\sim$ 3.86 h of follow-up observations between MJD 57798 and 58152, PSR J1831−04 has yet to be redetected. The folded discovery observations of PSRs J1812−15 and J1831−04 showing the acceleration in each pulsar can be found in Fig. 5.

Efforts to determine the full orbital solutions of both PSR J1812−15 and PSR J1831−04 have been hindered by the fact that in addition to being in binary systems, both pulsars also appear to exhibit nulling behaviour, with changes between 'on' and 'off' states having been observed in both pulsars. The lack of any detection of PSR J1831−04 since its initial discovery suggests that it may belong in the class of so-called 'intermittent' pulsars whose 'off' time-scales may range from hours to days and even years, and of which only a handful of examples are currently known (see e.g. Kramer et al. 2006a; Camilo et al. 2012; Lorimer et al. 2012; Lyne et al. 2017). As our understanding of the nulling time-scales of PSR J1812−15 still remains incomplete, it is possible that this pulsar may also qualify as intermittent, with non-detections sometimes appearing to last longer than the pulsar's typical integration time ($\sim$10−30 min).

A rudimentary estimate of the nulling fraction (NF) of each pulsar (the fraction of time each pulsar spends in its 'off' state)

Table 9. Parameters of the glitch observed in PSR J1706−4434. Values in parentheses represent standard 1σ uncertainties on the final digit as determined by TEMPO2. In the case of the permanent spin frequency derivative increment $\Delta\dot{\nu}$, an uncertainty of $3\,\sigma$ is provided as the upper limit.

Glitch parameters for PSR J1706−4434	
Estimated glitch epoch (MJD)	57601
Phase increment, $\Delta\phi$	0.085(13)
Permanent spin-frequency increment, $\Delta\nu$ (Hz)	$2.21(2) \times 10^{-8}$
Permanent spin-frequency derivative increment, $\lvert\Delta\dot{\nu}\rvert$ (s^{-2})	$<3.25 \times 10^{-17}$

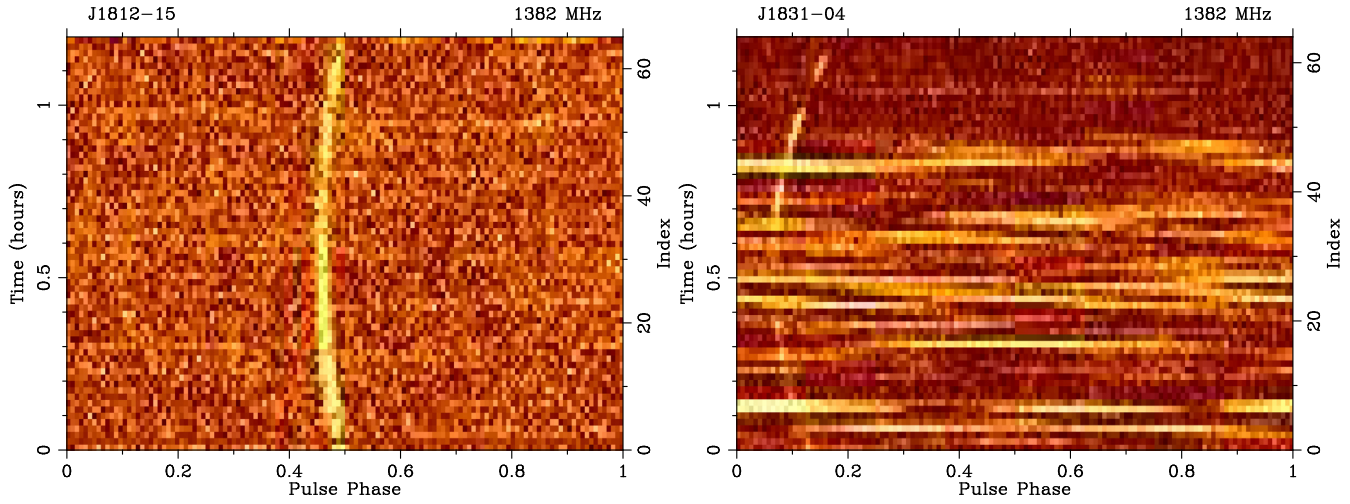

Figure 5. The discovery observations of PSRs J1812−15 (left) and J1831−04 (right). In both cases, these observations have been folded at a constant spin period and with an acceleration of $a = 0\,\mathrm{m\,s^{-2}}$. Even with the strong RFI present in the observation of PSR J1831−04, both pulsars show clear evidence of acceleration (indicated by the parabolic curvature of each pulsar's phase over time), suggesting the presence of binary motion. There is some evidence for a brief null in PSR J1831−04 approximately 1 h into the observation.

was conducted by visually inspecting each folded observation, in a method analogous to that described by Lyne et al. (2017). Intervals during which the pulsar was unambiguously detectable were classified as 'on', while all other intervals were classified as 'off'. The provided error σ on each NF is the standard error for a randomly sampled data set with n samples:

$$\sigma = \sqrt{\frac{\mathrm{NF}\,(1 - \mathrm{NF})}{n}}. \tag{8}$$

The calculated NF's for PSRs J1812−15 and J1831−04 are given in Table 10. It should be noted that all observations of PSR J1812−15 after MJD 58013 were recorded in fold mode using a fixed spin period. Should the binary orbit of the pulsar be more extreme than anticipated, this may also account for a portion of the observed non-detections, lowering the pulsar's true NF.

5.8 PSR J1822–0902, a pulsar with significant timing noise

PSR J1822−0902 is notable in that it possesses a high spin-down rate of approximately $\dot{P} = 1.778\,09(8) \times 10^{-14}$, implying both a young characteristic age τ_c and a high spin-down luminosity $\dot{E}$. In fact, PSR J1822−0902's estimated characteristic age of $\tau_c = 0.132\,\mathrm{Myr}$ ranks as the smallest value of τ_c among the pulsars presented in this paper, while its $\dot{E} = 2.13 \times 10^{35}\,\mathrm{erg\,s^{-1}}$ ranks as the highest. In addition, PSR J1822−0902 displays a significant degree of timing noise, requiring the use of additional spin derivative terms to model its observed behaviour. At present, attempts to model this timing noise as the result of either parallax (unlikely given the large DM-distance estimates listed in Table 4), proper motion or binary motion have been unsuccessful. It would therefore appear likely that this timing noise is intrinsic to the pulsar.

5.9 PSR J1810–1709, a nulling pulsar

With a DM of $\sim 670\,\mathrm{cm^{-3}\,pc}$, PSR J1810−1709 immediately stands out due to the presence of what may be a scattering tail in its profile, as seen in Fig. 2. Alternatively it may be that the pulsar simply has a wide inherent pulse profile, although some amount of scattering is likely given the high DM. Future multifrequency or wide-band observations of this pulsar may be useful in investigating the role played by scattering in the profile of this pulsar.

One feature that is not immediately evident from the pulsar profile is the nulling behaviour exhibited by PSR J1810−1709. Unlike the other variable pulsars we report in this paper, the 'on' and 'off' time-scales of PSR J1810−1709 appear to be much shorter. The average nulling and emission time-scales are 333 and 135 s respectively, with corresponding standard deviations of 291 and 122 s. All of these values are of the order of 100–300 pulse periods. With reference to the definition provided in Section 5.7, this would appear to classify PSR J1810−1709 as a nulling pulsar (as opposed to an intermittent pulsar). Once again, we calculate an NF (given in Table 10) by adopting the same method as described

Table 10. Parameters of four newly discovered pulsars which display either nulling or intermittent behaviour. For each pulsar, the span over which suitable observations are available, the number of observations and the total integration time are provided. The nulling fraction and its uncertainty is calculated according to the description in Section 5.7.

PSR name	Observing span (MJD)	Num. observations	Total integration time (h)	NF (per cent)
J1810−1709	55926−58407	5	3.5	70 (20)
J1812−15	55845−58298	48	18.0	54 (7)
J1831−04	55923−58152	18	4.8	79 (10)
J1854−0524	56028−57609	10	4.2	72 (14)

in Section 5.7, using the limited amount of search mode data recorded with the Parkes radio telescope.

5.10 PSR J1854–0524, a potentially intermittent pulsar

The one feature of note regarding PSR J1854−0524 is its apparent variability. Although approximately monthly confirmation observations commenced on MJD 57405, it was not until MJD 57554 that the pulsar was redetected, and not until MJD 57609 that an observation was recorded with sufficient S/N so as to be able to grid the pulsar's position. Using the same method as described in Section 5.7, we are able to derive an estimate of the pulsar's NF as provided in Table 10. As the longest non-detection of this pulsar exceeds 30 min, it may be that PSR J1854−0524 can also be classed among the intermittent pulsars, although further study of its 'on' and 'off' timescales will be required before a conclusive determination can be made.

6 COMPARISON TO THE KNOWN PULSAR POPULATION

We round out this paper with an updated comparison of the discoveries of the HTRU-S LowLat pulsar survey to the known pulsar population within the survey region. We therefore consider the 100 pulsars reported both here and in Ng et al. (2015). For the 40 pulsars reported in this paper, we use the parameters listed in Section 4, with the exception of PSR J1757−1854, whose parameters are given in Cameron et al. (2018). For the remaining 60 pulsars, we use the parameters listed in Ng et al. (2015), with the exception of PSR J1755−2550, whose parameters are taken from Ng et al. (2018). For the population of known pulsars, we have used the same set of pulsars within the survey region in each analysis, with their parameters taken from PSRCAT. However, as each known pulsar may not have a full set of available parameters, the number of known pulsars used will vary between analyses.

For the 64 pulsars in the HTRU-S LowLat survey population with well-constrained values of P and $\dot{P}$, Fig. 6 shows their positions on a P–$\dot{P}$ diagram as compared to 817 previously known pulsars within the survey region. It would seem from Fig. 6 that the HTRU-S LowLat pulsars represent a generally older, more-evolved collection of pulsars. This trend appears to be shared between the discoveries reported from both portions of the survey processing, however as just under half of the reported discoveries lack a well-measured $\dot{P}$, the possibility remains that this apparent trend may be the result of small-number statistics, a caveat which will apply throughout this section.

6.1 Distance

As described in Section 4, we estimate the distance to each of the 100 HTRU-S LowLat pulsars via their measured DM values, using

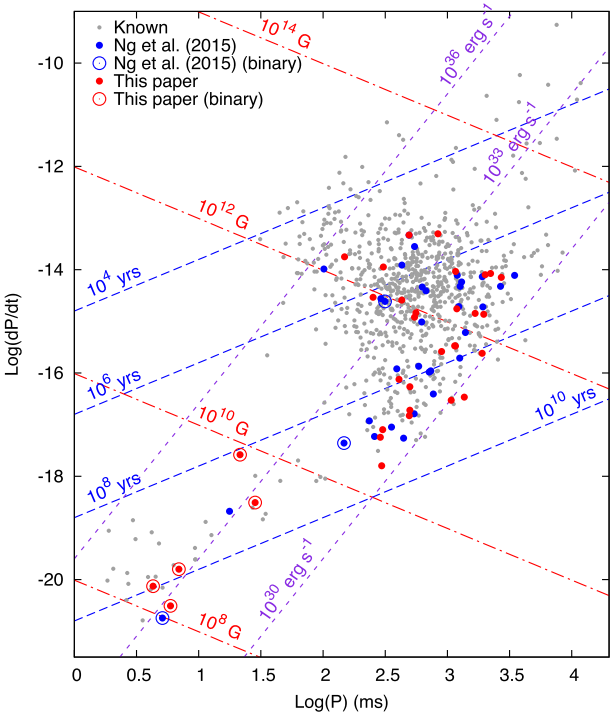

Figure 6. A P–$\dot{P}$ diagram displaying 64 HTRU-S LowLat discoveries with well-constrained P and $\dot{P}$ against the known Galactic pulsar population within the survey area. The 31 solved pulsars from Ng et al. (2015) are shown in blue, while the 33 solved pulsars from Tables 4, 5, and 6 are shown in red. Grey points represent the population of 817 known pulsars within the survey region. Circled points indicate binary pulsars.

independent estimates from both the NE2001 (Cordes & Lazio 2002) and YMW16 (Yao et al. 2017) electron density models. As per Ng et al. (2015), a typical uncertainty of 25 per cent is assumed for the NE2001 distance estimates, while Yao et al. (2017) report a typical uncertainty of ∼ 10 per cent for distance estimates from the YMW16 model. Note that it is not the intent of this comparison to render an assessment of the accuracy of either of these models, but in light of the statistical uncertainties involved in pulsar distance estimation, it is prudent to consider both of them.

Contrary to Ng et al. (2015), who reported the discovery of no pulsars within a distance less than ∼ 2 kpc, we report the discovery of two such nearby pulsars. PSR J1753−28, with a DM of only 18.0(9) cm^{-3} pc and a DM distance of 0.6–0.7 kpc, ranks as the closest pulsar discovered in the HTRU-S LowLat survey. Meanwhile PSR J1514−5316, with a DM of only 27.1(3) cm^{-3} pc and a DM distance of ∼ 0.9 kpc, comes in at a close second. This would indicate an approximate fraction of 'nearby' pulsars discovered within the survey of ∼ 2 per cent which, accounting

for small-number statistics, is consistent with the ∼ 3.8 per cent expectation value calculated by Ng et al. (2015).

A more comprehensive assessment of the degree to which the distances of the HTRU-S LowLat pulsars correspond to those of the overall Galactic population can be made with a Kolmogorov–Smirnov (KS) test. Distance statistics of the known pulsars within the survey region were compiled from PSRCAT. Where precision distance measurements were unavailable from PSRCAT, DM-distance estimates were calculated once again using both the NE2001 and YMW16 models, giving two data sets consisting of distance estimates for 835 known pulsars. The distance statistics of the HTRU-S LowLat and known populations were then compared on a per-model basis.

In both cases, the null hypothesis (that the distribution of distances derived for the 100 HTRU-S LowLat discoveries is drawn from the same population distribution as the known pulsars) cannot be ruled out. The YMW16 test results in a p-value of ∼0.3, while the NE2001 test results in a p-value of ∼0.6, with the p-value indicating the probability of the null hypothesis being correct. It would therefore appear that the distances of the HTRU-S LowLat pulsars are consistent with the background population. This consistency is shown in Fig. 7, which shows the similarities in the distance distributions of the two populations for both the NE2001 and YMW16 models both in terms of their respective histograms and cumulative distribution functions (CDFs).

6.2 Luminosity

At present, 81 of the HTRU-S LowLat pulsars have calibrated flux density measurements at 1.4 GHz. Using the distance estimates described in Section 6.1, it is therefore possible to also conduct a population analysis based on luminosity. This analysis was conducted against a background population of 748 known pulsars within the survey area which also have measured 1.4 GHz flux density values. Fig. 8 shows a comparison of these two populations, with distances and luminosities determined using both the NE2001 and YMW16 models. Note that the luminosity values (as listed here in Table 2) should be treated with a degree of caution, as they rely on both the uncertainties of the measured flux density of each pulsar as well as its DM distance estimates (see Section 6.1).

From both the NE2001 and YMW16 luminosity estimates shown in Fig. 8, it can clearly be seen that the HTRU-S LowLat survey has met its objective of uncovering pulsars at the lower end of the luminosity distribution. This is verified by a KS test, which shows that for both the NE2001- and YMW16-based luminosity estimates, the probability of the HTRU-S LowLat luminosity distribution having being drawn from the background pulsar distribution is less than 0.0001 per cent.

This result, although still somewhat preliminary, becomes more significant when considered together with the results of Section 6.1. That is, we have clearly discovered pulsars with lower luminosities across all distance scales, while sampling the same distance distribution as that of the background pulsars. This would seem to imply that we have yet to reach a 'bottom' of the luminosity distribution, and that even lower-luminosity pulsars are likely to still exist. This appears to be true even in the case of nearby pulsars, whose numbers one might naively expect to be exhausted first. Were this not the case, we should expect to see a growing bias in our discovered population towards larger distances when compared against the background population. Bolstering this conclusion are the particular examples of PSR J1514−5316, which has an estimated luminosity of only $\sim 0.1\,\mathrm{mJy\,kpc^2}$ under both the NE2001 and YMW16 models and ranks as the lowest-luminosity pulsar of the HTRU-S LowLat population by at least a factor of 2, and the binary MSP PSR J2322−2650, a recent discovery of HTRU-S HiLat (Spiewak et al. 2018) whose luminosity at 1.4 GHz and DM distance estimates appear extremely similar to PSR J1514−5316. It will likely fall to the next generation of radio telescopes such as MeerKAT, FAST, and the SKA, to continue the exploration into just how low the pulsar luminosity distribution truly extends.

6.3 Characteristic age

A further comparison can be performed using the characteristic age distribution of the HTRU-S LowLat pulsars. As per Lorimer & Kramer (2005), the characteristic age τ_c is derived from measurements of P and $\dot{P}$, therefore only those pulsars for which these values are both well measured are considered in this analysis. Similarly, as τ_c becomes contaminated as a result of the recycling process, only unrecycled pulsars [here defined as those pulsars for which the surface magnetic field $B_{\mathrm{surf}} < 3.0 \times 10^{10}$ G in order to remain consistent with the analysis performed by Ng et al. (2015)] are considered. These requirements leave a total of 56 HTRU-S LowLat pulsars and a background population of 756 known pulsars.

A KS test between these two distributions (as shown in Fig. 9) shows that they are not consistent with being drawn from the same population, to within a probability of < 0.001 per cent. From both of these side-by-side comparisons, it is clear that the sample of HTRU-S LowLat pulsars does indeed represent an older population of pulsars, with no unrecycled pulsar yet having a $\tau_c \leq 0.1$ Myr (a frequent definition of a 'young' pulsar). This reinforces a trend in the HTRU-S LowLat pulsar population first noted by Ng et al. (2015), and stands in opposition to the earlier prediction of Bates et al. (2012) who, after similarly not discovering any young, unrecycled pulsars in the HTRU-S MedLat survey, predicted that such pulsars would likely be uncovered by HTRU-S LowLat due to its higher sensitivity. It is possible that this result may still be attributable to the ambiguities of small-number statistics, and continued timing of the remaining unrecycled and unsolved pulsars will assist in further clarifying this result.

7 SURVEY YIELD EVALUATION

As noted previously, the processing of the HTRU-S LowLat survey now stands at ∼ 94 per cent. Therefore, it is now possible to conduct a near-full evaluation of the yield of both the survey and its first-pass processing pipeline with respect to both earlier predictions and the earlier analysis carried out by Ng et al. (2015). Keith et al. (2010) estimated that 957 'normal' pulsars (defined for this analysis as pulsars with $P > 30$ ms in order to maintain consistency with earlier analyses) should be detected by the HTRU-S LowLat survey, while Ng et al. (2015) later revised this estimate to 1020 normal pulsars. As these two results are statistically consistent, the latter is adopted to maintain consistency with the earlier yield analysis in Ng et al. (2015). Rescaling this estimate to account for the small proportion of the survey yet to be processed and reviewed results in a final estimate of ∼960 normal pulsars which ought to have been detected by current processing.

By comparison, as reported in Section 3, a total of 649 unique pulsars were redetected in the processed ∼ 94 per cent of the HTRU-S LowLat survey, of which 631 are normal pulsars. This is in addition to the 58 normal pulsars reported by Ng et al. (2015) and the 34 normal pulsars reported here, giving a total of 723 normal

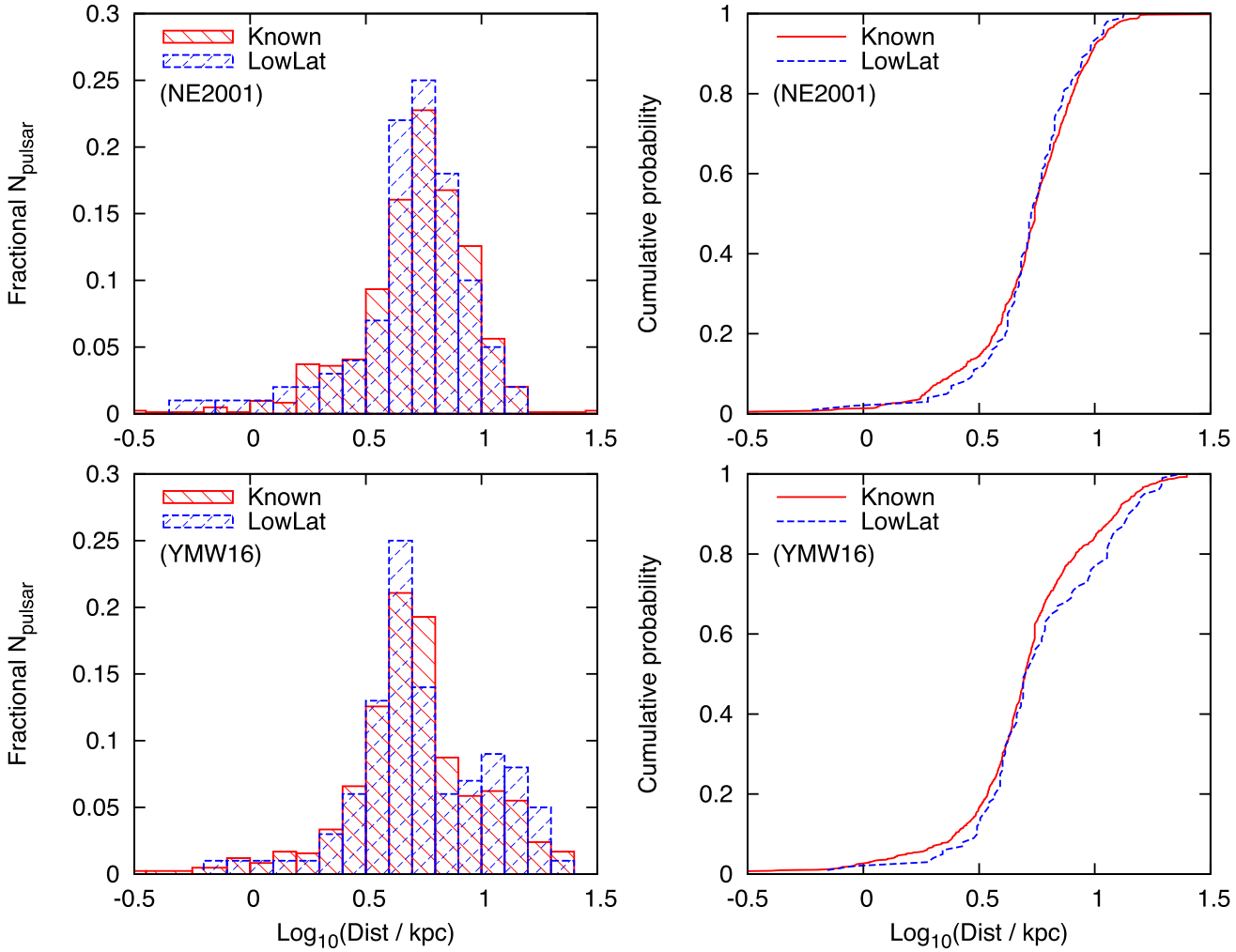

Figure 7. Distance distributions of the 100 HTRU-S LowLat pulsars (blue) and 835 previously known Galactic pulsars (red). Shown on the left are histograms of the distance distributions of each population under both the NE2001 (top) and YMW16 (bottom) models, normalized by the number of pulsars in each distribution and with a binsize of 0.1. Shown on the right are the corresponding CDFs of each distribution, again featuring the NE2001 (top) and YMW16 (bottom) models.

pulsar detections. Evidently, this falls short of the projected ∼960 detections by a factor of ∼ 25 per cent. This result also stands in contrast to the earlier evaluation of Ng et al. (2015), who predicted an expectation of 470−510 normal pulsar detections from the initial survey processing and reported a consistent 485 normal pulsar detections. The apparently lower detection rate in the portion of the survey data processed in this paper is in part due to a common set of pulsars which were detected in both processed portions (as noted previously in Section 3), although this cannot fully account for the discrepancy between the predicted and actual number of detected normal pulsars.

Separate predictions were also produced for the MSP population (here defined as $P \leq 30$ ms again in order to maintain consistency with earlier analyses), as these pulsars represent a distinct population which in turn is subject to different selection biases in a blind pulsar survey. Keith et al. (2010) and Ng et al. (2015) respectively predicted 51 and 43 MSP detections for the HTRU-S LowLat survey region, while an in-depth study by Levin et al. (2013) predicted a higher MSP yield of 68. Taking the lower and upper limits of these estimates and rescaling to account for the ∼ 94 per cent completion of the survey processing gives a final estimate of 40−64 expected MSP detections. By comparison, only 18 of the redetected pulsars outlined in Section 3 meet the $P \leq 30$ ms criteria, along with 2 pulsars reported by Ng et al. (2015) and 6 additional pulsars reported here. This gives a total of only 26 MSP detections from HTRU-S LowLat, a factor of 1.5−2.5 lower than predicted.

Multiple potential reasons exist as to why our detections of both normal pulsars and MSPs have fallen below their initial predictions. With respect to the MSP population, Ng et al. (2015) and Eatough et al. (2013) have already put forward a number of potential causes, including a limited understanding of the underlying Galactic MSP population leading to inadequate model estimates, detectability limitations due to scatter broadening, and the inability of our segmented search technique to take advantage of the fully-coherent sensitivity of each 72-min observation. While the discovery of PSR J1757−1854 shows the strengths of our segmented search pipeline in being able to detect pulsars with short, highly accelerated orbits, other similar pulsars such as PSRs J1802−2124 and J1141−6545 may still have been missed for the reasons discussed in Section 3.2. Therefore, the implementation of a fully coherent

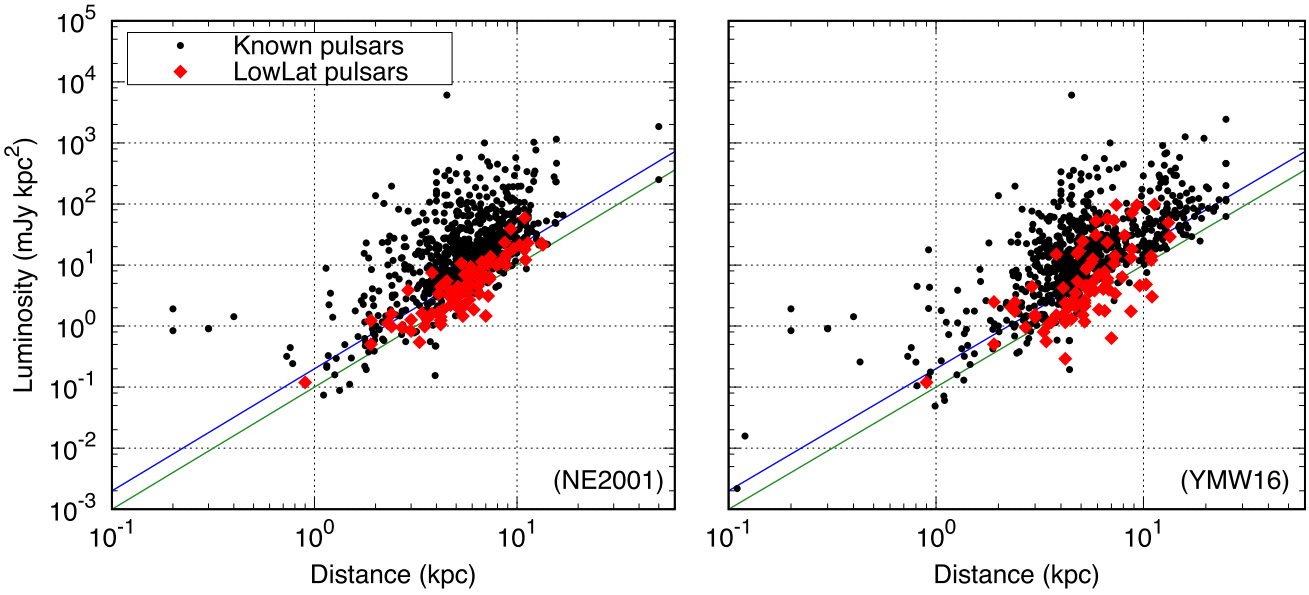

Figure 8. A comparison of the distances and 1.4-GHz luminosities of the 81 HTRU-S LowLat pulsars with calibrated flux densities to the background pulsar population. HTRU-S LowLat pulsars are shown in red, while the 748 known pulsars within the survey region are shown in black. The green and blue lines represent lines of constant 1.4-GHz flux density at 0.1 and 0.2 mJy, respectively. Where more accurate distances are unavailable, distances and luminosities are estimates using the NE2001 (left) and YMW16 (right) electron density models.

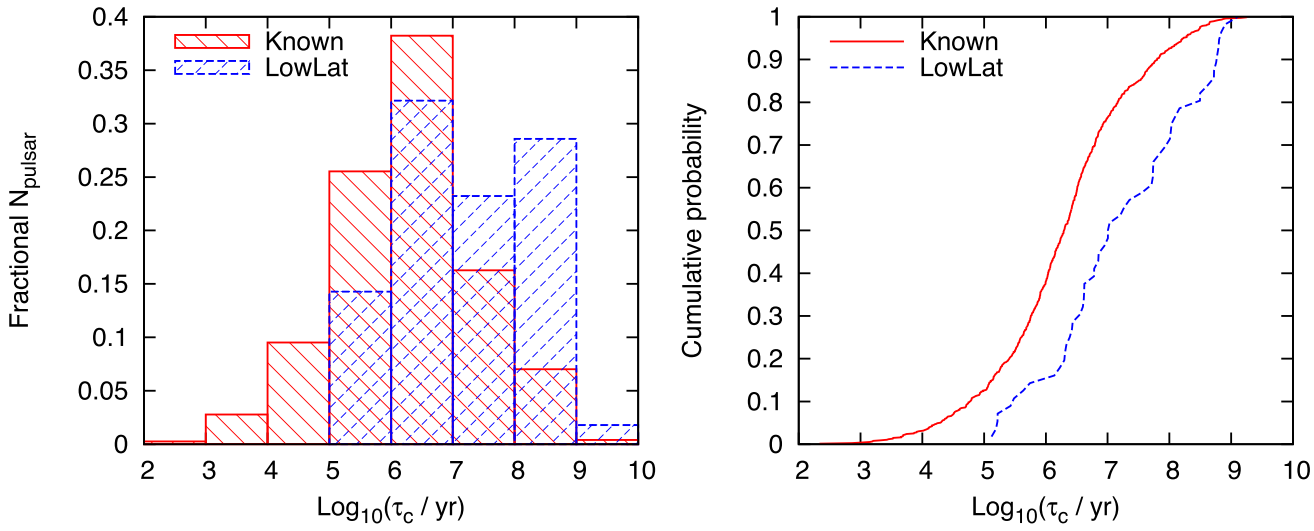

Figure 9. Characteristic age (τ_c) distributions of the 56 HTRU-S LowLat pulsars (blue) and 756 previously known Galactic pulsars (red) with well-constrained values of P and $\dot{P}$. Shown on the left are the histograms of the τ_c distributions of each population, normalized by the number of pulsars in each distribution and with a binsize of 1.0. Shown on the right are the corresponding CDFs of each τ_c distribution.

binary search remains an ongoing goal of the future reprocessing of this survey.

Additional factors exist which are likely to influence the lack of detections of both normal pulsars and MSPs. Nulling and intermittency, often factors in longer-period pulsars (see e.g. Biggs 1992), remain unavoidable obstacles in blind pulsar surveys. That being said, the 72-min integration times of the HTRU-S LowLat survey have been able to partially mitigate this effect, with at least six either nulling or intermittent pulsars and at least three eclipsing pulsars having been discovered so far. The influence of RFI also remains an ongoing problem, as despite our use of multiple RFI mitigation techniques, it accounted for a significant fraction of the candidates reported by the search pipeline. In particular, certain beams of the MB20 receiver would often experience extended spans of worsened interference, indicating potential hardware problems which multibeam RFI excision techniques would be unable to correct for. However, while RFI is likely to have contributed to a degraded survey sensitivity, its influence remains difficult to quantify.

Another limitation lies in the inherent shortcomings of Fourier-based search techniques. For example, the increase in Fourier power caused by red noise contamination (a consequence of our long integration times) is likely to mask the presence of longer-period pulsars in a Fourier-based search, as highlighted by Lazarus et al.

(2015). Fourier searches also lose sensitivity due the fact that they are an incoherent search technique, and are only able to sum a limited number of harmonics, resulting in the loss of additional Fourier power. This is especially true in the case of long-period or narrow duty-cycle pulsars, for which additional S/N can be attained once the candidate is folded at the correct period. Lazarus et al. (2015) further demonstrated that in the case of the Pulsar Arecibo L-band Feed Array survey (PALFA; Cordes et al. 2006), a significant loss of sensitivity was experienced for pulsars with $P > 100$ ms, becoming especially noticeable for pulsars with $P > 1$ s, with approximately 35 per cent of simulated pulsars remaining undetected. The synthetic profile injection technique used by Lazarus et al. (2015) in evaluating this loss in sensitivity may be useful in more thoroughly evaluating the limitations in the Fourier transform search technique specific to the HTRU-S LowLat data set. However, such an analysis lies beyond the scope of this paper, and may be included in a future publication.

One technique which may be able to counter these limitations of Fourier-based search techniques is that of the 'Fast Folding Algorithm' (FFA, Staelin 1969). Following recent in-depth studies of the FFA (see e.g. Kondratiev et al. 2009; Cameron et al. 2017), an implementation of the FFA is now being used as part of a new processing pass of the HTRU-S LowLat survey. Additionally, folding of candidates with lower Fourier significance may also reveal new candidates whose detectability was otherwise affected by the limitations of incoherent harmonic summing. Both of these techniques have already produced a handful of additional pulsar discoveries which will be the subject of a future publication. It is too soon to know to what extent these new discoveries will be able to bridge the gap between the expected and actual numbers of pulsars both detected and newly discovered in the HTRU-S LowLat survey. However, it is clear that the HTRU-S LowLat survey will remain a valuable resource for the application of future algorithms and for the verification of pulsars detected in future surveys.

8 ADDITIONAL DISCUSSION AND CONCLUSIONS

The HTRU-S LowLat pulsar survey was undertaken with the twin primary goals of discovering short-P_b, relativistic binary pulsars, as well as pulsars situated at the low end of the luminosity distribution. From the results presented both here and in Ng et al. (2015), which span the discovery of 100 new pulsars, it is clear that the survey has been successful on both counts. While PSR J1757−1854 is the only relativistic binary to have been discovered by the survey, as many as 12 other binary systems have also been discovered, verifying our sensitivity to binary systems. Meanwhile Section 6.2 clearly indicates that the discovered pulsars sit lower on the luminosity distribution function than the general background population within the survey region, and suggests that there are pulsars with even lower luminosities yet to be discovered. These achievements come as a direct consequence of the longer integration times, larger bandwidth and finer time resolution employed by this survey in comparison to previous search efforts such as those undertaken with the PMPS, as well as our implementation of the 'partially coherent segmented acceleration search' technique.

However, it is clear that there remains room for improvement. For example, although our pipeline only missed approximately 2 per cent of the known pulsar population, the examples of PSRs J1435−6100 and J1810−2124 in Section 3.2 and the lower than anticipated survey yield show that there remains parameter spaces to which the pipeline is insensitive. Therefore, in addition to completing the processing of the entire survey with the segmented pipeline to ensure a consistent first-pass processing, future processing should focus on resolving these known shortcomings. This should include the development and implementation of a fully coherent binary search (e.g. a 'jerk' search), as well as an implementation of the FFA. With these and other modifications, it is likely that reprocessing of the HTRU-S LowLat survey will continue to yield new results for many years to come. Even with the ongoing Survey for Pulsars and Extragalactic Radio Bursts (SUPERB; Keane et al. 2018) and the advent of the next generation of pulsar surveys which will be enabled by telescopes such as MeerKAT, FAST, and the SKA, the steady production of new pulsar discoveries and other key scientific results from the multiple reprocessings of the PMPS (see e.g. Keane et al. 2010; Eatough et al. 2010, 2013) clearly demonstrates the value in reprocessing legacy surveys with a variety of search techniques.

In addition to having met its broad scientific goals, we have also reported the discovery of a number of scientifically-interesting pulsars from the HTRU-S LowLat survey, many of which are likely to require continuing observation in order to fully exploit their scientific potential. For example, the three MSP-WD binary systems (PSRs J1537−5312, J1547−5709, and J1618−4624) add to the collective picture of MSP evolution, with the latter of these presenting lingering questions with regards to its evolutionary history and whether it should be classed as the result of either Class A or Class C RLO. Ongoing observations of PSR J1618−4624 (especially with an increase in sensitivity) may lead to an eventual Shapiro measurement of the system should its inclination be sufficiently high, helping to resolve this ambiguity via a measurement of the pulsar mass. Meanwhile, the observed glitch in PSR J1706−4434 may not have been an isolated event, and ongoing monitoring may detect the presence of additional glitches, contributing further to the body of knowledge regarding glitching pulsars. If PSR J1706−4434 is seen to glitch regularly, higher cadence observations may be warranted so as to better localize each glitch in time as it occurs and hopefully measure the presence of the exponential relaxation in spin period which is typically observed immediately following a glitch event.

Future work will need to focus on developing timing solutions for those pulsars which remain unsolved. This will both help to understand the individual properties of these pulsars, but will also assist in characterizing the discovered population as a whole. In the case of PSR J1653−45, ongoing monitoring with high cadence bursts of observations as the pulsar passes into and out of its eclipse state will be critical in helping to constrain the pulsar's orbital and timing solution. For the black widow PSR J1745−23, high-cadence observations spanning several orbits within a time-scale of days or weeks will be critical in obtaining an initial orbital solution, and a timing model such as the BTX model (see e.g. Shaifullah et al. 2016) will likely be required to handle the long-timescale orbital variabilities inherent in a black widow system. Finally, in the cases of PSRs J1812−15 and J1831−04, the development of binary and timing solutions will require as high a cadence of follow-up observations as can be justified in order to successfully detect them during their 'on' phase. While this is likely to be an easier endeavour in the case of PSR J1812−15 given its lower NF, it is important that both of these pulsars eventually be solved, as along with PSR J1653−45, they represent a rarer class of long-P binary pulsar. Given the significant accelerations detected in both PSR J1812−15 and PSR J1831−04, and an inferred P_b range for each pulsar of the order of days to weeks (based on equation 1), it is possible that both PSR J1812−15 and PSR J1831−04 may represent objects of some

scientific interest at the very least in terms of their evolutionary history.

ACKNOWLEDGEMENTS

The Parkes Observatory is part of the Australia Telescope National Facility which is funded by the Australian Government for operation as a National Facility managed by the Commonwealth Scientific and Industrial Research Organisation (CSIRO). Pulsar research at the Jodrell Bank Centre for Astrophysics and the observations using the Lovell Radio Telescope are supported by a consolidated grant from the Science and Technology Facilities Council in the UK. This work was supported by the Australian Research Council (ARC) Centres of Excellence CE110001020 (CAASTRO) and CEA0100004 (OzGrav). Survey processing resources were provided by the Australian National Computational Infrastructure (NCI) high-performance computing centre at the Australian National University (ANU) in association with CAASTRO, and by the Max Planck Computing and Data Facility (MPCDF). The authors wish to thank Paulo Freire and Alessandro Ridolfi for their instruction and advice regarding techniques for pulsar solving and timing, Thomas Tauris for his discussions and insight into binary pulsar evolution, Eleni Graikou for her instruction on data calibration techniques, Ralph Eatough for his support and advice regarding the operation of the segmented search pipeline, and Hasan Aslan and Malte Klasing for their assistance in pulsar candidate classification. The authors further wish to acknowledge the assistance of Kira Kühn, Andreas Schmidt and the staff of the MPCDF, and Sally Cooper and the staff of the Jodrell Bank Center for Astrophysics in creation of a new tape archive copy of the HTRU-S LowLat survey at the MPCDF, which was vital in allowing for the processing and results presented in this paper. ADC acknowledges the support of both the International Max Planck Research School (IMPRS) for Astronomy and Astrophysics at the Universities of Bonn and Cologne, and the Bonn-Cologne Graduate School of Physics and Astronomy (BCGS). We further acknowledge that these results are based upon work initially presented in Cameron (2018). However, this paper represents a significant update, and should be seen as superseding this earlier doctoral work.

REFERENCES

Abdo A. A. et al., 2013, ApJS, 208, 17
Backer D. C., 1975, A&A, 43, 395
Barr E. D. et al., 2013, MNRAS, 435, 2234
Bassa C. G. et al., 2016, MNRAS, 456, 2196
Bates S. D. et al., 2012, MNRAS, 427, 1052
Bates S. D., Lorimer D. R., Rane A., Swiggum J., 2014, MNRAS, 439, 2893
Belczynski K., Kalogera V., Bulik T., 2002, ApJ, 572, 407
Bhat N. D. R., Bailes M., Verbiest J. P. W., 2008, Phys. Rev. D, 77, 124017
Biggs J. D., 1992, ApJ, 394, 574
Burgay M. et al., 2003, Nature, 426, 531
Cameron A. D., 2018, PhD thesis, Universität Bonn
Cameron A. D., Barr E. D., Champion D. J., Kramer M., Zhu W. W., 2017, MNRAS, 468, 1994
Cameron A. D. et al., 2018, MNRAS, 475, L57
Camilo F., Manchester R. N., Gaensler B. M., Lorimer D. R., 2002, ApJ, 579, L25
Camilo F., Ransom S. M., Halpern J. P., Reynolds J., 2007, ApJ, 666, L93
Camilo F., Ransom S. M., Chatterjee S., Johnston S., Demorest P., 2012, ApJ, 746, 63
Champion D. J. et al., 2016, MNRAS, 460, L30
Cieślar M., Bulik T., Osłowski S., 2020, MNRAS, 492, 4043
Cordes J. M., Lazio T. J. W., 2002, preprint (arXiv:e-print)
Cordes J. M. et al., 2006, ApJ, 637, 446
Demorest P. B., Pennucci T., Ransom S. M., Roberts M. S. E., Hessels J. W. T., 2010, Nature, 467, 1081
Eatough R. P., Molkenthin N., Kramer M., Noutsos A., Keith M. J., Stappers B. W., Lyne A. G., 2010, MNRAS, 407, 2443
Eatough R. P., Kramer M., Lyne A. G., Keith M. J., 2013, MNRAS, 431, 292
Faucher-Giguère C.-A., Kaspi V. M., 2006, ApJ, 643, 332
Frail D. A., Goss W. M., Whiteoak J. B. Z., 1994, ApJ, 437, 781
Freire P. C. C., 2005, in Rasio F. A., Stairs I. H., eds, ASP Conf. Ser. Vol. 328, Binary Radio Pulsars. Astron. Soc. Pac., San Francisco, p. 405
Freire P. C. C., Ridolfi A., 2018, MNRAS, 476, 4794
Freire P. C. C., Camilo F., Kramer M., Lorimer D. R., Lyne A. G., Manchester R. N., D'Amico N., 2003, MNRAS, 340, 1359
Gelfand J. D., Gaensler B. M., Slane P. O., Patnaude D. J., Hughes J. P., Camilo F., 2007, ApJ, 663, 468
Gonthier P. L., Harding A. K., Ferrara E. C., Frederick S. E., Mohr V. E., Koh Y.-M., 2018, ApJ, 863, 199
Graikou E., Verbiest J. P. W., Osłowski S., Champion D. J., Tauris T. M., Jankowski F., Kramer M., 2017, MNRAS, 471, 4579
Green D. A., 2019, Journal of Astrophysics and Astronomy, 40, 36
Gullón M., Miralles J. A., Viganò D., Pons J. A., 2014, MNRAS, 443, 1891
Haslam C. G. T., Klein U., Salter C. J., Stoffel H., Wilson W. E., Cleary M. N., Cooke D. J., Thomasson P., 1981, A&A, 100, 209
Hobbs G. B., Edwards R. T., Manchester R. N., 2006, MNRAS, 369, 655
Hotan A. W., van Straten W., Manchester R. N., 2004, PASA, 21, 302
Johnston H. M., Kulkarni S. R., 1991, ApJ, 368, 504
Johnston S., Manchester R. N., Lyne A. G., Bailes M., Kaspi V. M., Qiao G., D'Amico N., 1992, ApJ, 387, L37
Keane E. F., Ludovici D. A., Eatough R. P., Kramer M., Lyne A. G., McLaughlin M. A., Stappers B. W., 2010, MNRAS, 401, 1057
Keane E. F. et al., 2018, MNRAS, 473, 116
Keith M. J. et al., 2010, MNRAS, 409, 619
Keith M. J. et al., 2012, MNRAS, 419, 1752
Kondratiev V. I., McLaughlin M. A., Lorimer D. R., Burgay M., Possenti A., Turolla R., Popov S. B., Zane S., 2009, ApJ, 702, 692
Kramer M., Lyne A. G., O'Brien J. T., Jordan C. A., Lorimer D. R., 2006a, Science, 312, 549
Kramer M. et al., 2006b, Science, 314, 97
Lazaridis K. et al., 2011, MNRAS, 414, 3134
Lazarus P. et al., 2015, ApJ, 812, 81
Levin L. et al., 2013, MNRAS, 434, 1387
Li D. et al., 2018, IEEE Microw. Mag., 19, 112
Lin J., Rappaport S., Podsiadlowski P., Nelson L., Paxton B., Todorov P., 2011, ApJ, 732, 70
Lorimer D. R., 2011, Astrophysics Source Code Library, record ascl:1107.016
Lorimer D. R., Kramer M., 2005, Handbook of Pulsar Astronomy. Cambridge Univ. Press, Cambridge
Lorimer D. R., Bailes M., McLaughlin M. A., Narkevic D. J., Crawford F., 2007, Science, 318, 777
Lorimer D. R., Lyne A. G., McLaughlin M. A., Kramer M., Pavlov G. G., Chang C., 2012, ApJ, 758, 141
Lyne A. G. et al., 2004, Science, 303, 1153
Lyne A. G. et al., 2017, ApJ, 834, 72
Manchester R. N. et al., 2001, MNRAS, 328, 17
Manchester R. N., Hobbs G. B., Teoh A., Hobbs M., 2005, AJ, 129, 1993
McLaughlin M. A. et al., 2006, Nature, 439, 817
Middleditch J., Kristian J., 1984, ApJ, 279, 157
Ng C. et al., 2015, MNRAS, 450, 2922
Ng C. et al., 2018, MNRAS, 476, 4315
Phinney E. S., Verbunt F., 1991, MNRAS, 248, 21
Prinz T., Becker W., 2015, preprint (arXiv:1511.07713)
Ransom S. M., 2001, PhD thesis, Harvard University
Ransom S. M. et al., 2011, ApJ, 727, L16
Roberts M. S. E., 2013, in van Leeuwen J., ed., Proc. IAU Symp. 291, Neutron Stars and Pulsars: Challenges and Opportunities after 80 years. Cambridge University Press, Cambridge, UK, p. 127

Shaifullah G. et al., 2016, MNRAS, 462, 1029
Smith D. A. et al., 2019, ApJ, 871, 78
Spiewak R. et al., 2018, MNRAS, 475, 469
Staelin D. H., 1969, IEEE Proc., 57, 724
Staveley-Smith L. et al., 1996, PASA, 13, 243
Sutton J. M., 1971, MNRAS, 155, 51
Tauris T. M., 2011, in Schmidtobreick L., Schreiber M. R., Tappert C., eds, ASP Conf. Ser. Vol. 447, Evolution of Compact Binaries. Astron. Soc. Pac., San Francisco, p. 285
Tauris T. M., Savonije G. J., 1999, A&A, 350, 928
Tauris T. M., van den Heuvel E. P. J., 2014, ApJ, 781, L13
Tauris T. M., Langer N., Kramer M., 2011, MNRAS, 416, 2130
Tauris T. M., Langer N., Kramer M., 2012, MNRAS, 425, 1601
Thornton D. et al., 2013, Science, 341, 53
Thorsett S. E., Chakrabarty D., 1999, ApJ, 512, 288
Tiburzi C. et al., 2013, MNRAS, 436, 3557
van Straten W., Bailes M., 2011, PASA, 28, 1
Weltevrede P. et al., 2010, ApJ, 708, 1426
Wenger M. et al., 2000, A&AS, 143, 9
Yan W. M. et al., 2011, Ap&SS, 335, 485
Yao J. M., Manchester R. N., Wang N., 2017, ApJ, 835, 29

SUPPORTING INFORMATION

Supplementary data are available at *MNRAS* online.

Table A1. 755 redetections of 390 pulsars recorded during processing of the 44 per cent of the HTRU-S LowLat survey as reported in this paper.

Please note: Oxford University Press is not responsible for the content or functionality of any supporting materials supplied by the authors. Any queries (other than missing material) should be directed to the corresponding author for the article.

APPENDIX: PREVIOUSLY KNOWN PULSARS WITHIN THE SURVEY REGION

A1 Redetections

As described in Section 3, 755 individual redetections of 390 were made as part of the survey processing reported in this paper. We list the details of all 755 redetections in Table A1 (full version available as Supporting Information with the online version of the paper).

A2 Non-detections

As per Section 3.1, 21 non-detections spanning 21 unique known pulsars were encountered by the partially coherent segmented acceleration search pipeline. These pulsar non-detections are listed in Table A2, along with the beam, angular offset (θ), the expected S/N (S/N_{exp}) and the PSRCAT spin period P_{cat} and DM_{cat}. For each non-detection, a manual fold of the relevant beam using the current PSRCAT ephemeris of the pulsar was also conducted. In 18 cases this manual analysis resulted in a redetection of the pulsar, with the resulting S/N_{eph} also listed in Table A2. While 9 of these non-detections have yet to be accounted for, the remaining 12 can be explained as follows:

(i) PSRs J1322−6329, J1501−5637, J1709−4342, and J1733−2837 all suffered from the influence of significant RFI in their corresponding observations, such that additional cleaning of the data beyond the standard RFI mitigation employed by our pipeline was required to redetect the pulsar.

(ii) PSR J1550−5418, a magnetar also known as AXP 1E 1547.0−5408, is known to experience significant radio variability including spans of apparent non-emission (Camilo et al. 2007), accounting for its non-detection both by the pipeline and the later ephemeris fold.

(iii) PSR J1709−4401 has been previously described by Tiburzi et al. (2013) as an 'intermittent' pulsar. Were it observed during an 'off' state, this would account for its non-detection both by the pipeline and the later ephemeris fold.

(iv) PSRs J1524−5819 and J1611−4811 were both redetected by the ephemeris fold, but with $S/N_{eph} < S/N_{min}$. Therefore, the non-detection by the search pipeline of these two pulsars is not unexpected. Similarly, the ephemeris fold of PSR J1509−5850 only resulted in $S/N_{eph} = 9.4$ which, while technically above the S/N_{min}, is sufficiently close that it can likely be grouped into this category.

(v) PSR J1747−2958 was discovered by Camilo et al. (2002) in a search of the Mouse Nebula. Its interaction with this nebula, combined with a relatively-low DM, makes it susceptible to scintil-

Table A1. 755 redetections of 390 pulsars recorded during processing of the 44 per cent of the HTRU-S LowLat survey as reported in this paper. Listed for each redetection are the beam in which the detection was made (identified by a UTC time stamp and beam number), the Galactic longitude (l) and latitude (b) of the pulsar, the offset between this position and the centr of the telescope beam (θ), the observed spin period (P_{obs}) and DM (DM_{obs}) of the pulsar, the expected apparent flux density of the pulsar given by to equation (5) (S_{exp}), the expected S/N of the pulsar as given by equation (7) (S/N_{exp}), and finally the observed S/N of the pulsar (S/N_{obs}). The following is a sample of the full table, which is available as Supporting Information with the online version of the paper.

PSR name	Pointing/beam	l (°)	b (°)	θ (°)	P_{obs} (ms)	DM_{obs} (cm^{-3} pc)	S_{exp} (mJy)	S/N_{exp}	S/N_{obs}
B1011−58	2012-09-05-20:01:28/04	283.706	−2.144	0.17	819.924	379.0	0.361	108.0	83.9
B1015−56	2012-07-23-23:59:36/09	282.732	0.341	0.11	503.462	433.2	1.540	354.0	265.3
B1030−58	2012-09-24-21:37:39/04	285.907	−0.980	0.19	464.210	415.2	0.151	38.6	40.2
B1030−58	2012-09-23-22:09:55/05	285.907	−0.980	0.24	464.210	416.6	0.052	13.4	17.5
B1044−57	2012-08-05-00:16:37/10	287.065	0.733	0.20	369.427	239.4	0.143	25.3	26.9
B1044−57	2012-09-05-21:14:20/08	287.065	0.733	0.12	369.428	240.0	0.527	92.8	89.7
B1046−58	2012-08-02-06:52:42/07	287.425	0.577	0.28	123.714	128.3	0.103	15.7	38.4
B1046−58	2012-08-05-00:16:37/03	287.425	0.577	0.12	123.714	127.8	3.170	484.0	498.7
B1046−58	2012-08-05-00:16:37/10	287.425	0.577	0.38	123.714	129.3	0.004	0.5	41.9
B1046−58	2012-09-24-03:00:15/10	287.425	0.577	0.19	123.714	128.3	1.080	139.0	231.7

Table A2. Pulsars with $S/N_{exp} > S/N_{min} = 9$ which were not detected in the ∼ 44 per cent of the HTRU-S LowLat survey processed by the partially coherent segmented acceleration search pipeline for this paper. Listed is the telescope beam of each non-detection (identified by a UTC time stamp and beam number), along with the offset (θ) of the pulsar from the centre of the beam, the PSRCAT values of spin period (P_{cat}) and dispersion measure (DM_{cat}), the expected S/N of the pulsar as estimated from the radiometer equation as described in Section 3 (S/N_{exp}), and the S/N resulting from a fold of beam using the PSRCAT ephemeris of the pulsar (S/N_{eph}).

PSR name	Pointing/beam	θ (°)	P_{cat} (ms)	DM_{cat} (cm^{-3} pc)	S/N_{exp}	S/N_{eph}	Comments
J1031−6117	2012-07-18-05:13:39/07	0.12	306.411	506.8	10.5	12.7	Weak, close to beam FWHM, but unambiguous in ephemeris fold.
J1233−6344	2012-04-01-10:19:04/02	0.094	756.892	495.0	11.7	12.4	Weak, but unambiguous in ephemeris fold.
J1301−6310	2011-12-22-15:34:56/09	0.075	663.830	86.1	17.8	15.1	XRS (Prinz & Becker 2015). Unambiguous in ephemeris fold.
J1309−6526	2012-04-14-10:01:12/03	0.091	398.292	340.0	20.3	10.8	Weak detection.
J1322−6329	2012-04-05-14:47:06/10	0.096	2764.209	659	26.6	13.0	Significant RFI contamination. Pulsar only detectable in ephemeris fold after additional cleaning.
J1501−5637	2011-12-13-18:40:47/11	0.11	782.949	258.0	18.2	11.0	Significant RFI contamination.
J1509−5850	2012-04-03-19:16:00/03	0.094	88.922	140.6	13.4	9.4	HE pulsar (Weltevrede et al. 2010). Weakly detected in ephemeris fold, close to S/N_{min}.
J1524−5819	2012-08-01-10:10:14/07	0.096	961.043	406.6	15.9	8.8	Weakly detected in ephemeris fold, below S/N_{min}.
J1550−5418	2011-07-14-05:40:23/01	0.022	2069.833	830.0	114.0[a]	–	Magnetar, AXP 1E 1547.0−5408 (Camilo et al. 2007).
J1611−4811	2011-12-27-19:03:07/08	0.047	1296.850	221.0	12.4	8.6	Weakly detected in ephemeris fold, below S/N_{min}.
J1633−4805	2011-12-30-19:34:06/13	0.096	710.830	1120.0	15.0	14.4	Unambiguous in ephemeris fold.
J1709−4342	2011-12-12-05:16:53/02	0.10	1735.898	281.0	15.7	17.0	RFI contamination.
J1709−4401	2012-09-24-06:43:27/01	0.026	865.235	225.8	233.0	–	Described as 'intermittent' (Tiburzi et al. 2013).
J1733−2837	2011-12-07-03:42:23/03	0.070	768.185	225.0	14.4	15.5	Significant RFI contamination.
J1738−3107	2011-12-22-22:10:51/03	0.10	549.498	735.0	19.3	12.3	Weak, but unambiguous in ephemeris fold.
J1747−2958	2012-08-03-09:31:42/08	0.061	98.814	101.5	21.0	–	Discovered by Camilo et al. (2002) with $S_{1400} = 0.25$ mJy. Associated with the Mouse Nebula, with flux variability likely due to interstellar scintillation. Also undetected by Ng et al. (2015).
J1755−2534	2012-07-26-12:48:29/02	0.12	233.541	590.0	10.6	11.6	Weak, close to beam FWHM, but unambiguous in ephemeris fold.
J1801−2115	2012-03-30-22:36:23/01	0.078	438.113	778.8	14.3	10.2	Weak detection.
J1819−1131	2012-08-05-08:17:44/02	0.069	1388.137	578.0	17.7	11.4	Weak, but unambiguous in ephemeris fold. Possible red noise confusion.
J1819−1717	2012-07-26-14:01:59/03	0.12	393.522	405.0	14.9	14.6	Unambiguous in ephemeris fold.
J1822−1617	2012-07-25-14:25:48/12	0.064	831.156	647.0	11.3	10.2	Wide pulse profile with $\delta \simeq 14$ per cent, appears to be scattered.

Note. [a]For pulsars with no published pulse width, an effective pulse width of $W_{eff} = P_{cat}/2$ is used to calculate S/N_{exp}.

lation. Apparent flux variability due to this effect has already been observed in this pulsar's discovery observations. PSR J1747−2958 was also not detected by Ng et al. (2015), and remains undetectable here even after the ephemeris fold.

(vi) With a relatively-long catalogue period of $P_{cat} = 1388$ ms and an S/N_{eph} significantly weaker than its S/N_{exp}, the non-detection of PSR J1819−1131 is attributed to likely confusion with red noise, reducing its detectability in the Fourier domain.

(vii) The profile of PSR J1822−1617 displays a wide pulse shape with a duty cycle of $\delta \simeq 14$ per cent and evidence of a scattering tail, consistent with its high DM. This wide profile, in combination with a weak ephemeris fold of $S/N_{min} = 10.2$, may have contributed the pulsar's non-detection.

A3 Binary redetections

As per Section 3.2, 17 unique binary pulsars were redetected across 28 individual survey beams. Table A3 lists the highest S/N detections of each pulsar in each searched segment of each beam, along with the detected acceleration (a), the catalogue orbital period (P_b) and eccentricity (e) of each binary as well as the calculated limiting accelerations (a_{max} and a_{min}) along the line of sight at the epoch of each observation.

For those pulsars detected in multiple segments of the same beam, the S/N of the detection in each subsequent segment falls by roughly $\sqrt{2}$ as the lengths of the segments are halved until the pulsar falls below the survey noise floor and is rendered undetectable. This general trend is subject to a number of minor caveats:

(i) Due to the fact that, as listed in Table 1, the quarter-length segments were often only searched at $500\,m\,s^{-2} > |a| > 200\,m\,s^{-2}$ (much higher than the a_{max} or a_{min} of the pulsars listed in Table A3), the detections in the quarter-length segments typically break this trend with significantly reduced S/N values.

(ii) The full-length detections of PSRs J1216−6410 and J1748−3009 were made at harmonics, reducing their apparent S/N.

In addition, while the majority of the accelerations reported in Table A3 are consistent with the calculated acceleration limits of a_{max} and a_{min}, the increasingly large ambiguity of $\dot{P}$ which occurs over shorter integration lengths (an effect exacerbated by weak pulsar detections) means that some reported acceleration values

Table A3. Redetections of binary pulsars from ∼ 44 per cent of the HTRU-S LowLat survey. Each redetected pulsar is listed along with its PSRCAT values of orbital period P_b and eccentricity e, and the observed spin period P_{obs} and DM_{obs}. Also listed are the calculated maximum and minimum values of acceleration (a_{max} and a_{min}, respectively) along the line of sight at the epoch of each beam in which the pulsar was redetected (identified by a UTC time stamp and beam number). The redetections with the highest S/N from each segment group (and their corresponding acceleration a) are also reported.

PSR name	P_b (h)	e	a_{max} (m s^{-2})	a_{min} (m s^{-2})	Pointing/beam	P_{obs} (ms)	DM_{obs} (cm^{-3} pc)	Full-length S/N	Full-length a (m s^{-2})	Half-length S/N	Half-length a (m s^{-2})	Quarter-length S/N	Quarter-length a (m s^{-2})	Eighth-length S/N	Eighth-length a (m s^{-2})
B1800−27	9672.7	0.00051	0.0006	−0.0006	2011-12-11-05:59:48/03	334.420	161.3	-[b]	–	29.9	−2.1	18.9	−232.7	17.7	−23.6
					2012-10-01-06:42:41/10	334.412	165.0	54.8	−0.2	41.0	1.0	16.9	−211.4	23.6	−6.6
B1820−11	8586.3	0.79	0.005	−0.006	2011-12-23-01:58:46/13	279.821	428.0	91.2	0.6	65.6	0.03	28.2	206.4	34.0	−23.6
					2011-12-31-00:27:33/12	279.824	416.5	16.1	−0.7	13.5	−2.1	–	–	–	–
					2012-07-22-12:33:52/09	279.837	424.9	14.2	0.3	12.4	2.1	–	–	–	–
J1822−0848	6883.9	0.059	0.002	−0.002	2012-04-02-18:07:28/13	2504.472	189.7	18.6	−0.2	13.4	−17.0	–	–	–	–
					2012-04-12-17:41:06/13	2504.459	185.5	67.0	0.06	47.4	3.1	27.3	202.1	25.6	−40.7
J1740−3052	5544.7	0.58	0.07	−0.08	2012-07-21-10:23:16/05	570.380	738.0	83.2	−0.5	59.9	0.03	21.0	−202.9	32.3	−6.6
J1751−2857	2657.9	0.00013	0.004	−0.004	2012-12-14-00:34:43/05	3.915	43.0	16.0	0.06	14.9	0.03	–	–	–	–
J1125−5825	1833.7	0.00026	0.009	−0.009	2011-10-04-20:14:39/07	3.102	124.9	20.9	0.0	14.9	0.03	–	–	–	–
					2011-12-20-18:13:43/06	3.102	124.9	17.5	0.0	12.7	0.03	–	–	–	–
					2011-12-27-13:47:20/07	3.102	124.9	24.8	0.0	17.7	0.03	–	–	–	–
J1727−2946	967.4	0.046	0.06	−0.06	2011-10-12-03:10:49/04	27.086	61.3	15.1	0.0	11.3	0.03	–	–	–	–
J1811−1736	450.7	0.83	0.98	−4.8	2011-12-31-22:59:57/01	104.148	475.2	40.5	0.9	29.4	0.03	11.3	202.1	16.0	−6.6
J1454−5846	298.2	0.0019	0.27	−0.27	2012-12-30-17:34:08/06	45.244	115.6	19.9	−0.2	14.6	0.03	–	–	–	–
J1811−2405	150.5	0.0000016	0.23	−0.23	2012-08-05-14:33:10/04	2.661	60.8	24.9	0.3	22.1	0.03	–	–	–	–
J1337−6423	114.8	0.00002	0.91	−0.91	2012-01-02-01:12:28/09	9.425	259.3	16.5	0.6	–	–	–	–	–	–
J1216−6410	96.9	0.0000068	0.29	−0.29	2012-04-13-09:24:34/09	3.540	47.4	35.4[a]	0.0	41.2	0.03	–	–	24.0	−6.6
J1748−3009	70.4	0	0.24	−0.24	2012-11-30-04:17:16/08	19.367	418.6	11.7[a]	0.06	–	–	–	–	–	–
J1431−5740	65.4	0.0000043	0.48	−0.48	2011-12-23-16:52:20/07	4.111	131.3	18.7	0.3	12.4	0.03	–	–	–	–
J1435−6100	32.5	0.000011	5.3	−5.3	2011-12-14-19:52:54/06	9.351	114.1	–	–	20.9	−3.2	–	–	14.2	−6.6
					2011-12-22-16:53:19/07	9.350	114.1	–	–	12.5	3.1	–	–	–	–
J1802−2124	16.8	0.0000025	12.1	−12.1	2011-10-12-04:24:15/07	12.649	149.9	–	–	16.6	11.6	–	–	–	–
					2011-12-30-23:14:07/02	12.652	148.9	12.9	1.1	17.0	3.1	–	–	–	–
J1141−6545	4.7	0.17	56.5	−108.9	2012-02-18-20:27:49/05	394.152	114.8	191.5	−1.0	285.9	−7.4	123.1	−202.9	162.7	−40.7
					2012-02-18-20:27:49/11	394.029	118.2	–	–	12.7	−80.8	–	–	–	–
			57.5	−108.2	2012-07-23-00:10:48/07	394.034	114.8	31.0	−0.7	46.7	−77.6	23.7	−198.7	28.2	−6.6
					2012-07-23-00:10:48/08	394.151	117.1	13.3	0.6	18.3	−9.6	8.7	−202.9	10.8	−6.6

Notes. [a]Indicates that the highest S/N detection for that segment was found at a harmonic.
[b]The full-length segment for beam 2011-12-11-05:59:48/03 suffered a processing error, resulting in the non-detection of B1800 − 27 in this segment.

may exceed these limits. This effect is most prominent in the eighth-segment detections given their short duration of only $t_{\rm int} = 9$ min.

A similar effect can be seen in PSR J1141−6545 where for the two beams from each pointing in which the pulsar was detected, a discrepancy exists between the two reported half-length acceleration values. This is likely a result of the pulsar's long spin period which, as with decreasing $t_{\rm int}$, increases the ambiguity of the measured $\dot{P}$ and hence also increases the ambiguity of the measured value of a. This effect can also be seen in the half-length detection of PSR J1822−0848 in beam 2012-04-02-18:07:28/13.

[1]*Max-Planck Institut für Radioastronomie, Auf dem Hügel 69, D-53121 Bonn, Germany*
[2]*CSIRO Astronomy & Space Science, Australia Telescope National Facility, PO Box 76, Epping, NSW 1710, Australia*
[3]*Centre for Astrophysics and Supercomputing, Swinburne University of Technology, Mail H39, PO Box 218, VIC 3122, Australia*
[4]*ARC Center of Excellence for Gravitational Wave Discovery (OzGrav), Swinburne University of Technology, Mail H11, PO Box 218, VIC 3122, Australia*
[5]*ASTRON, the Netherlands Institute for Radio Astronomy, Postbus 2, NL-7990 AA Dwingeloo, the Netherlands*
[6]*Jodrell Bank Center for Astrophysics, University of Manchester, Alan Turing Building, Oxford Road, Manchester M13 9PL, UK*
[7]*International Centre for Radio Astronomy Research, Curtin University, Bentley, WA 6102, Australia*
[8]*INAF – Osservatorio Astronomico di Cagliari, Via della Scienza 5, I-09047 Selargius (CA), Italy*
[9]*Center for Gravitational Waves and Cosmology, West Virginia University, Chestnut Ridge Research Building, Morgantown, WV 26505, USA*
[10]*Department of Physics and Astronomy, University of British Columbia, 6224 Agricultural Road, Vancouver, BC V6T 1Z1, Canada*
[11]*Department of Physics, Universitá di Cagliari, S.P. Monserrato-Sestu Km 0,700, I-09042 Monserrato, Italy*
[12]*Centre d'Études Nucléaires de Bordeaux Gradignan, IN2P3/CNRS, Université Bordeaux 1, BP120, F-33175 Gradignan Cedex, France*
[13]*Institute for Radio Astronomy & Space Research, Auckland University of Technology, Private Bag 92006, Auckland 1142, New Zealand*
[14]*Fakultät für Physik, Universität Bielefeld, Postfach 100131, D-33501 Bielefeld, Germany*

This paper has been typeset from a TEX/LATEX file prepared by the author.